This is a preprint, the final version is subject to change, of the American Mineralogist (MSA)
Cite as Authors (Year) Title. American Mineralogist, in press.
(DOI will not work until issue is live.) DOI: http://dx.doi.org/10.2138/am-2017-6154

REVISION 2

Multiple-reaction geobarometry for olivine-bearing igneous rocks

Ziberna Luca[1,*], Green Eleanor C.R.[2], Blundy Jon D.[1]

[1] School of Earth Science, University of Bristol, BS8 1RJ Bristol, United Kingdom

[2] Institute of Geochemistry and Petrology, ETH Zurich, 8092 Zurich, Switzerland

*Corresponding author (present address: luca.ziberna@uni-bayreuth.de; Bayerisches Geoinstitut, University of Bayreuth, 95440 Bayreuth, Germany)

Abstract

Efforts to map the vertical distribution of mafic and ultramafic igneous rocks in the Earth's crust and uppermost mantle have long been hampered by the lack of precise geobarometers for the appropriate mineral assemblages. The average pressure (avP) method (Powell and Holland 1994, Am Min 79, 120-133) is a multiple-reaction approach that uses a least-squares minimization to average the pressures derived from individual mineral equilibria, taking into account both their uncertainties and correlations. We applied avP to a carefully selected database of published phase equilibrium experiments in dry to H_2O-saturated, andesitic to basaltic and peridotitic systems at P = 0.6–9.3 kbar, T = 940–1240˚C, with log fO_2 from NNO - 2.6 to NNO + 3.6 log units (where NNO is nickel-nickel oxide buffer). We made minor modifications to the thermodynamic models of clinopyroxene, spinel and olivine in order to improve the accuracy and precision of the results given by the avP method. Tests on the experimental database, using the modified thermodynamic models and spinel + clinopyroxene + olivine + plagioclase equilibria, showed that avP can reproduce the experimental P, within the calculated 1σ uncertainties (0.9–2.6 kbar; 1.6 kbar on average), for 67% of the database. No systematic deviations of the calculated pressure (P) with temperature (T) or mineral compositions are observed. Given the large compositional range of the experimental database, these results suggest that the method can be applied

to any gabbroic, pyroxenitic or peridotitic rocks that contain the appropriate phase assemblage clinopyroxene + olivine + plagioclase ± spinel. For assemblages equilibrated at $P < 5$ kbar, the calculated P shows a slight dependence on T, which therefore needs to be well constrained in order to keep the overall P uncertainties as low as possible. T can be estimated using either available independently-calibrated geothermometers or a simple calculation routine suggested in this work. Application of avP to gabbroic xenoliths from Dominica, Lesser Antilles, and to gabbroic and peridotitic xenoliths from Wikieup, Arizona, demonstrates the ability of the method to produce precise P estimates for natural assemblages equilibrated at both mid and lower crustal conditions respectively. Depending on the errors on mineral composition, appropriateness of the T estimate and attainment of equilibrium of the assemblage, P uncertainty for natural rocks is ≤ 1.0 kbar. Such level of precision can help discriminating rival petrogenetic processes in subduction zone, intra-plate and mid oceanic ridge settings.

Keywords

Geobarometry, Phase equilibria, Mafic crust, Gabbros, Peridotites

Introduction

Estimating the pressure (P) and temperature (T) of formation of mafic and ultramafic igneous rocks is a fundamental step in studying the evolution of magmatic systems and the thermal and lithological structure of the crust and crust-mantle transition zone. Developing accurate and precise thermobarometric methods for such rocks is therefore critically important. Conventional methods use phase compositions combined in either empirical or theoretical formulations to derive expressions for P and T, with the fundamental assumption that the assemblage of interest attained equilibrium. Commonly used geothermometers and geobarometers for gabbroic and peridotitic rocks are based on

single reactions between mineral end-members, often derived by simple regressions of experimental data. Examples include two-pyroxene thermometers (e.g., Wells 1977; Putirka 2008) and barometers (Putirka 2008), olivine-pyroxenes-plagioclase barometers (e.g., Fumagalli et al. 2017), hornblende-plagioclase thermobarometers (e.g., Holland and Blundy 1994; Molina et al. 2015) and magnetite-ilmenite thermometers (e.g., Ghiorso and Evans 2008). Empirical methods based on the composition of a single mineral phase, such as clinopyroxene barometers (e.g., Nimis 1995; Putirka 2008) and amphibole thermobarometers (e.g., Ridolfi and Renzulli 2012) are also available for gabbroic as well as, basaltic and andesitic rocks. Mineral-melt thermobarometers potentially produce precise pressure and temperature estimates (Falloon et al. 2007; Putirka 2008; Putirka 2016a; Neave and Putirka 2017), but their application to gabbroic or peridotitic rocks is limited to assemblages containing melt in equilibrium with the solid phases (interstitial melt or trapped melt inclusions).

For any given plutonic suite, a barometer or thermometer should meet the following conditions: i) sufficient precision to discriminate between rival petrogenetic processes, ii) applicability over the *P*-*T* range of interest, iii) calibration for the compositions of interest, iv) consistency across the entire suite. Depending on the assemblage, criterion (i) can often be met for temperature, as model errors can be as low as 40 ºC (e.g., Putirka 2008), which is small relative to the range of formation of mafic/ultramafic plutonic rocks (800–1300 ºC). However, for existing barometers that are applicable to subsolidus gabbroic assemblages (e.g., two-pyroxene or single-clinopyroxene barometers of Putirka 2008, single-amphibole barometer of Ridolfi and Renzulli 2012), typical model errors are 3–4 kbar (inferred from experimental data not used in the calibration; see Putirka 2008, 2016b and Erdmann et al. 2014 for a review). This is unacceptably high considering the typical pressure range to be investigated (e.g., < 7 kbar for island arcs and intra-oceanic settings). For empirical or semi-empirical single-reaction thermobarometers, condition (ii) is usually met, as calibrant phase equilibrium experiments generally cover a wide range of *P* and *T* (e.g., 0–20 kbar, 800–1400ºC). Condition (iii) is particularly critical when adopting empirical or semi-empirical thermobarometry, because relationships that are too

73 simplified or that have no thermodynamic basis become unreliable when applied outside the range of
74 the calibration data. For the same reason, some empirical thermobarometers may be sensitive to the
75 buffering effect of phases that are not involved in the reaction, but are present in the assemblage,
76 hampering the application to natural samples with phase assemblages that differ from those in the
77 calibration dataset. This issue may be particularly important when single-phase empirical
78 thermobarometers calibrated using *suprasolidus* (i.e. melt-present) experiments (e.g., Ridolfi and
79 Renzulli 2012) are applied to plutonic rocks equilibrated at *subsolidus* (i.e. melt-absent) conditions.
80 Finally, condition (iv) may be difficult to meet when the rock suite includes samples with different
81 mineral assemblages, requiring the adoption of different, potentially inconsistent, single-reaction
82 thermobarometers calibrated on different experimental datasets.
83 A potential solution that fulfils all of the above conditions for pressure determination is multiple-
84 reaction barometry, employing an internally consistent dataset of thermodynamic data for mineral end-
85 members (e.g., Berman 1988; Holland and Powell 1998, 2011), along with a set of activity-
86 composition (*a*-*x*) relations calibrated for use with the same end-member dataset[1]. The multiple-
87 reaction method allows all of the *P* and *T* information in a mineral assemblage to be used
88 simultaneously, provided the necessary thermodynamic models exist, via an independent set of
89 reactions among the end-members of the phases (Berman 1991; Gordon 1992; Powell and Holland
90 1988, 1994, 2008). End-member thermodynamic data and activity-composition (*a*-*x*) relations are now
91 available for the majority of rock-forming minerals of the crust and shallow mantle (e.g., Ghiorso and
92 Sack 1995; Holland and Powell 2011; Diener et al. 2007; Green et al. 2007, 2012, 2016; Gualda et al.
93 2012; White et al. 2014; Jennings and Holland 2015), thus potentially allowing the method to be
94 applied consistently to rock suites across a wide range of mineralogy and composition.

[1] We use the term 'thermodynamic model' to refer to both the thermodynamic properties of the end-members and the constituent *a*-*x* relations

A single reaction among the end-members of phases is sufficient to calculate the value of *P* at given *T*. However, in a robust application of multiple-reaction barometry, there are several reactions forming an independent set, and the *P* values are statistically over-determined. Owing to the uncertainties in thermodynamic models and in analysed mineral compositions, the reactions do not, in general, intersect at the same *P*(*T*). Therefore a statistical approach is needed to calculate the optimal *P*. Such an approach must be weighted by the uncertainties affecting each reaction in the independent set, and this weighting must also take into account the correlated influence of these uncertainties on reactions that share end-members (Powell 1985; Powell and Holland 1994). The average *P* (avP) method (Powell and Holland 1988, 1994, 2008), is one of the few available algorithms for multiple-reaction thermobarometry that uses a rigorous statistical approach to handle both uncertainties *and* correlations. The algorithm is accessible via the software THERMOCALC, using the Holland and Powell (1985, 1990, 1998, 2011) internally consistent dataset of end-members and, in principle, any suitably encoded *a-x* relations with the modified regular solution formulations described in Powell and Holland (1993) and Holland and Powell (2003).

The avP algorithm in THERMOCALC has historically been applied to metamorphic rocks, and the development of *a-x* relations suitable for their use has concentrated on the metamorphic domain. However, following the work of Jennings and Holland (2015) and Green et al. (2016), a set of *a-x* relations is, for the first time, available for the phases expected in hydrous igneous rocks under crustal and upper mantle conditions. Given the potential of avP to fulfil all the conditions for optimal geobarometry, we evaluated the accuracy of the method and accompanying *a-x* relations for mafic and ultramafic rocks using a dataset of phase equilibrium experiments in basaltic and peridotitic systems, together with well-equilibrated natural samples, as a test case.

Methodological overview and rationale

Our aim is to develop a procedure for reliably applying multiple-reaction barometry to crustal-depth mafic and ultramafic igneous rocks. A database of phase equilibrium experiments (Supplementary Material 1) was used to evaluate the results obtained with THERMOCALC's avP algorithm (Powell and Holland 1988, 1994, 2008) and a selection of published thermodynamic models for mineral phases. The thermodynamic models were then refined, where necessary, to minimise systematic discrepancies between the avP calculations and the experimental database. Prior estimates of T and analytical or model uncertainty were explored, both for the experimental database, and for natural samples. Our work focused on rocks containing the assemblage SCOlP (see Table 1 for abbreviations). This assemblage is common in mafic and ultramafic plutonic rocks from a variety of tectonic settings, and appears in a relatively large number of experimental runs. We further tested avP calculations using the sub-assemblage COlP. This yields only three independent reactions, compared with six for SCOlP, and is therefore potentially less robust. However, COlP can be applied to a larger number of experiments and natural samples, including plagioclase peridotites.

Refinement of the thermodynamic models allows the avP approach to satisfy criteria (i) to (iii) above. Regarding criterion (iv), the method is devised such that it is possible to apply mutually consistent barometers across a suite of rocks, simply by adding further sets of well-calibrated a-x relations to those for olivine, clinopyroxene, plagioclase and spinel, using the same internally-consistent dataset of end-member thermodynamic properties (Holland and Powell 2011).

Supplementary Material 2 describes how to obtain software and input files for applying the avP approach to SCOlP and COlP assemblages, and provides an example calculation.

Experimental database

We assembled a database of published phase equilibrium experiments in natural andesitic to basaltic and peridotitic systems whose run products contain, at least, olivine, clinopyroxene and plagioclase. Some experimental datasets were excluded, despite containing the right assemblage, either because (i)

the experiments show clear evidence of disequilibrium (e.g., large compositional inhomogeneity of the run products, significant Fe loss), or (ii) run duration was very short (i.e. < 2 hours) or (iii) mineral compositions were not reported. A reference list of experiments that satisfied these requirements is reported in Supplementary Material 1 and their *P*-*T* conditions are shown in Figure 1. Clinopyroxenes in most of the experiments at $P \geq 9$ kbar and $T \geq 1150$˚C have low Ca contents (≥0.38 atoms per formula unit, apfu; Bartels et al. 1991; Draper and Johnston 1992; Kinzler and Grove 1992; Fig. 2a). The closure of the solvus separating low- and high-Ca pyroxene compositions is difficult to capture accurately in *a*-*x* modelling and, moreover, such low-Ca clinopyroxenes are rare in natural igneous rocks. We therefore excluded the experiments containing these clinopyroxenes from the dataset. Additionally, clinopyroxenes from atmospheric pressure experiments (0.001 kbar) show a range of tetrahedral aluminium (Al^{IV} = 2 – Si [apfu]) contents that exceeds that at higher pressures (Fig. 3), suggestive of a complex cation partitioning for 1-atm clinopyroxenes. Existing geobarometers involving Al- and Na-in-clinopyroxene components systematically fail to predict pressure for 1-atm experiments. This has been ascribed to Na-loss during the experiment (Putirka 2008), although, conversely, Mollo et al. (2010) showed that fast-growing clinopyroxene crystals contain excessive Na and Al, compensating for depletions in Si, Ca and Mg relative to the equilibrium composition. Considering that some equilibria used in this work involve Al and Na partitioning, we therefore removed all 1-atm experiments from the avP dataset. Additional filtering based on the quality of microprobe analyses and possible presence of aberrant data (see Supplementary Material 1) yielded a final dataset of 209 experiments with the COlP assemblage, of which 62 also contain the SCOlP assemblage.

The conditions covered by the refined experimental database are P = 0.5–9.3 kbar, T = 935–1240˚C (Fig. 1) and log fO_2 from NNO - 2.6 to NNO + 3.6 log units. Compositions of olivine, spinel, clinopyroxene and plagioclase are shown in Fig. 2. Olivines are almost pure solid solutions of forsterite

and fayalite, with only minor or trace amounts of Ca and Mn components (Ca < 0.025 apfu; Mn < 0.024 apfu). Plagioclases are solid solutions of albite and anorthite, with only minor amounts of K (< 0.12 apfu) and Fe_{tot} (< 0.09 apfu) components. Spinels show a wide range of composition including magnetites, ulvospinels and spinels sensu-stricto, with variable amounts of Cr (Fig. 2c) and mg# in the range 0.11-0.89. Clinopyroxenes are augites with variable Al (0.08–0.39 apfu) and Ti (0.00–0.10 apfu) and low Na (0.01–0.08 apfu). The 62 experiments containing the subset SCOlP cover roughly the same range of P-T conditions and mineral compositions (e.g., Figs. 1 and 2a,b), with log fO_2 from NNO -0.1 to NNO + 3.6.

Average-Pressure calculations: methodology

Overview of the avP method

An optimal value of P, $\overline{P}$, may be found by least-squares averaging of multiple independent phase equilibrium constraints, each of which can be formulated as a reaction between end-members. To find the optimal value is not simply a matter of averaging the values of the P_r, the pressures obtained from each reaction r in the set, because some end-members appear in more than one reaction. If the pressures of the reactions are adjusted to coincide at $\overline{P}$, the implication is that the calculated chemical potentials of the end-members are being adjusted. Adjustments to chemical potentials must be applied consistently across each of the end-member reactions, meaning that the reactions must be moved in a suitably correlated way in P space in order to coincide at $\overline{P}$. The approach is most powerful if applied via using a set of fully thermodynamic models for the phases, in which the chemical potentials of end-members are constructed from parameters representing other physical properties, such as standard enthalpies, within some uncertainty. In this case, the correlated adjustments to the P_r required to achieve coincidence at $\overline{P}$, can be made by adjusting the end-member properties, based on a covariance matrix that is known *a priori*. The method amounts to 'least-squares adjustment of indirect

189 observations' (e.g. Mikhail 1976). Such a method, the avP algorithm, is described in detail by Powell
190 and Holland (1988, 1994, 2008), and exploits the Holland and Powell (1990, 1998, 2011) dataset of
191 end-member thermodynamic properties, combined with a set of *a—x* relations for each solid solution to
192 describe the thermodynamics of mixing (Gordon 1992 discussed a similar procedure). The TWEEQU
193 thermobarometric method of Berman (1991) is of the same type, but does not account for the
194 correlations in the adjustments applied to the P_r.

195 A statement of equilibrium for each multiphase reaction, *r*, can be written as

196 $$\sum_i \nu_i \mu_i = \sum_i \nu_i \mu_i^0 + \mathrm{R}\ T \ln K_r = \Delta G_\mathrm{r}^\mathrm{o} + \mathrm{R}T\ln K_\mathrm{r} = 0, \quad (1)$$

197 where, for end-member i in a phase j of specified crystal structure, ν_i is the reaction coefficient, μ_i is
198 the total chemical potential and μ_i^0 is the chemical potential of the pure end-member at *P, T*. $\Delta G_\mathrm{r}^\mathrm{o}$ is the
199 Gibbs free energy difference in kJ for the reaction among the pure end-members, R is the gas constant
200 (0.0083144 kJ/K·mole) and K_r is the equilibrium constant, which is given by

201 $$K_r = \prod_i (a_i)^{\nu_i}, \quad (2)$$

202 a_i being the activity of end-member *i*.

203 The avP algorithm, as implemented in THERMOCALC (Powell and Holland 1988), finds the activities
204 of end-members given the observed compositions of the phases, at a likely P_0 and T_0 (initial estimates
205 of pressure and temperature), to compute each equilibrium constant K_r. Taking the corresponding
206 expression for $\Delta G_\mathrm{r}^\mathrm{o}$ from the Holland and Powell (1985 1990, 1998, 2011) dataset, it linearises
207 expression (1) at T_0, P_0, to form the equation from which *P* is obtained (Fig. 4):

208 $$\mathrm{a} + \mathrm{b}\ T_0 + \mathrm{c}\ P + \mathrm{R}T_0 \ln K_\mathrm{r} = 0 \quad (3)$$

209 The *a*, *b* and *c* terms represent the end-member enthalpy, entropy and volume changes, ΔH_r, $-\Delta S_r$ and
210 ΔV_r, respectively, for the reaction.

211 Uncertainties in equation (3) are derived from uncertainties in the properties of individual end-
212 members involved in the reaction. Only the enthalpies and activities of the end-members are considered

213 to be uncertain, since the Holland and Powell dataset treats end-member entropies and volumetric
214 properties as exact. The uncertainties in the end-member enthalpies are correlated with each other, and
215 their standard deviations and correlation coefficients are extracted from the Holland and Powell dataset.
216 The uncertainties in the activities of end-members are assumed to be independent of each other, and are
217 propagated through from (i) the analytical uncertainties in the compositional variables and (ii) the
218 uncertainties in the *a-x* relations, treated simply as uncertainties in the values of $W^{j}_{(m,n)}$.

219 As described in Powell and Holland (1988), the uncertainties in the enthalpies and activities of end-
220 members can be converted into uncertainties on the a and $\ln K_r$ terms of equation (3), taking into
221 account the reaction coefficient of each end-member. A full covariance matrix can ultimately be
222 derived, describing the uncertainties and correlations among the estimates of P from each of the
223 independent reactions (P_r).

224 Using the reactions and the corresponding covariance matrix, the avP algorithm finds an optimal
225 least-squares average of the P_r values, $\overline{P}$, with a well-defined uncertainty $\sigma_{\bar{P}}(T_0)$. Figure C2 from
226 Powell and Holland (1988) illustrates graphically how two correlated pressures (P_r) are combined to
227 give $\overline{P}$.

228 A number of diagnostic values are displayed following the avP procedure (see Supplementary
229 Material 2 and Powell and Holland, 1994), to assist meaningful application of the method. The
230 diagnostic value σ_{fit} is particularly helpful, providing a measure of how appropriately the pressure
231 information in the independent set of reactions can be combined. If σ_{fit} lies within the cut-off value
232 provided by the χ^2 test, representing 95 % confidence, then it is reasonable to assume that the selected
233 phases are indeed in thermodynamic equilibrium, given realistic uncertainties in the mineral analyses
234 and thermodynamic models.

235 **Independent reactions used in this work**

236 For each of the two assemblages (SCOlP and COlP) considered, we specified the independent set of

reactions to be used by the avP algorithm. These were chosen to have generally low uncertainties in their individual pressure estimations, *Pr*, implying that they are sensitive to pressure, and also to lie reliably within 20 kbar of the experimental pressures during model refinement. The choice of independent reactions affects the calculated $\overline{P}$, but the variation in $\overline{P}$ is of the order of $\sigma_{\overline{P}}$. For the assemblage SCOlP, the selected reactions are (see example in Supplementary Material 2 for ΔH_r, ΔS_r and ΔV_r for each reaction):

r1) cenh + cats = fo + an
$Mg_2Si_2O_6 + CaAl_2SiO_6 = Mg_2SiO_4 + CaAl_2Si_2O_8$

r2) cfs + cats = fa + an
$Fe_2Si_2O_6 + CaAl_2SiO_6 = Fe_2SiO_4 + CaAl_2Si_2O_8$

r3) cenh + jd = fo + abh
$Mg_2Si_2O_6 + NaAlSi_2O_6 = Mg_2SiO_4 + NaAlSi_3O_8$

r4) cenh + 2 cats = di + an + sp
$Mg_2Si_2O_6 + 2\ CaAl_2SiO_6 = CaMgSi_2O_6 + CaAl_2Si_2O_8 + MgAl_2O_4$

r5) cenh + jd + 2 herc = fa + abh + 2 sp
$Mg_2Si_2O_6 + NaAlSi_2O_6 + 2\ FeAl_2O_4 = Fe_2SiO_4 + NaAlSi_3O_8 + 2\ MgAl_2O_4$

r6) 2 cfs + 2 acm + herc = 2 fa + 2 abh + mt
$2\ Fe_2Si_2O_6 + 2\ NaFeSi_2O_6 + FeAl_2O_4 = 2\ Fe_2SiO_4 + 2\ NaAlSi_3O_8 + Fe_3O_4$

where the number of independent reactions is equal to $s - c$, with s being the number of end-members and c the number of components involved in mixing (see Table 2).

For COlP, an independent set contains three reactions. The natural choice is simply those of the set of reactions r1—r6 that do not involve end-members of spinel solid solution, i.e., reactions r1, r2 and r3.

Thermodynamic models

We employed the internally consistent thermodynamic dataset of Holland and Powell (2011; version 6.3, generated 29 March, 2016), and an initial selection of published *a—x* relations that are appropriate

for use with this dataset: the models for plagioclase, clinopyroxene, olivine and spinel were taken respectively from Holland and Powell (2003), Green et al. (2016), Hackler and Wood (1989), and Bryndzia and Wood (1990). Specifically, these *a—x* relations are regular solution models (one-parameter Margules solutions), with mixing on sites, allowing for asymmetry introduced via a van Laar parameter applied to each end-member.

During our development of a procedure for application of avP to igneous rocks, a major requirement was to make modifications to the thermodynamic models (end-member properties and/or *a—x* relations) in order to achieve accurate estimation of $\overline{P}$ values for our experimental database. Many of these modifications involved the adjustment of end-member Gibbs energy functions from the dataset, $G^{ds}(P,T)$, by functions $\Delta G^{mod}(P,T)$, such that for end-member *i*, $G_i(P,T) = G_i^{ds}(P,T) + \Delta G_i^{mod}(P,T) = G_i^{ds}(P,T) + a + b\,T + c\,P$ (the constants a, b and c may be considered to represent enthalpy, entropy and volume terms respectively). Additionally we made minor structural changes to the *a—x* relations, and adjusted some of the interaction energies, *W(m,n)*.

By repeatedly assessing the results of avP run on the experimental database as described below, we adopted the following thermodynamic models for clinopyroxene, olivine and spinel. We did not modify the Holland and Powell (2003) models for plagioclase, an asymmetric solution between high-albite, anorthite and sanidine. Model end-members are listed in Table 2, and a full description of the *a—x* relations and end-member thermodynamic data can be found in the Supplementary Material 3.

Clinopyroxene. The starting point for the clinopyroxene *a—x* relations was the 'augite model' of Green et al. (2016) that entails mixing of [Mg, Fe^{2+}, Al, Fe^{3+}] on the M1, [Na, Ca, Mg, Fe^{2+}] on the M2, and [Si, Al] on the tetrahedral sites. The end-members high-temperature clinoenstatite (cenh) and clinoferrosilite (cfs) do not appear in the Holland and Powell (2011) dataset, but are constructed by adding $\Delta G_i^{trans}(P,T)$ terms to the Gibbs energy functions for ortho-enstatite (en) and ortho-ferrosilite (fs) respectively (Green et al. 2016), where $\Delta G_i^{trans}(P,T)$ represents the Gibbs energy change of the

*Pbca—C*2/*c* transition. The model incorporates order-disorder of Fe^{2+}-Mg across M1 and M2, expressed via the proportions of an end-member fmc, $Fe^{M2}Mg^{M1}Si_2O_6$. Like the cenh and cfs end-members, the fmc end-member does not appear in the dataset, but has a Gibbs energy function that can be expressed as $\frac{1}{2}(G_{\mathrm{cenh}}(P,T) + G_{\mathrm{cfs}}(P,T)) + \Delta G^{\mathrm{od}}_{\mathrm{fmc}} = \frac{1}{2}(G^{\mathrm{ds}}{}_{\mathrm{en}}(P,T) + G^{ds}{}_{\mathrm{fs}}(P,T) + \Delta G_{en}{}^{trans}(P,T) + \Delta G_{fs}{}^{trans}(P,T)) + \Delta G^{\mathrm{od}}_{\mathrm{fmc}}$, where $\Delta G^{\mathrm{od}}_{\mathrm{fmc}}$ is the Gibbs energy change of ordering to form fmc from a disordered 1:1 mixture of cenh and cfs. The model also includes Si-Al order-disorder on the tetrahedral site, but whereas in Green et al. (2016) this order-disorder was expressed explicitly, by including both an ordered and a disordered Ca-tschermaks end-member in the solid solution, we here made a minor simplification by replacing the ordered and disordered Ca-tschermaks end-members with a single end-member, cats, from the Holland and Powell (2011) dataset, for which the thermodynamic properties reflect disordering with temperature. This makes negligible difference to the calculations.

Three problems that emerged during testing of the avP procedure were linked to the clinopyroxene model:

1) Calculations on the COlP assemblage tended to produce $\overline{P}$ estimates that exceeded experimental pressures by ~5 kbar.
2) The avP diagnostics (see Supplementary Material 2) for the calculations on the SCOlP assemblage suggested that the clinopyroxene end-members Ca-tschermaks and jadeite were particularly likely to exhibit large, uncertainty-normalised residuals in activity, e^*, and that cenh strongly influenced $\overline{P}$.
3) When $\overline{P}$ was calculated over a range of T_0, values of σ_{fit} and $\sigma_{\overline{P}}$ were typically smaller for small values of temperature, with minima occurring at temperatures < T_{exp}. This showed that the models' temperature-dependences were poorly calibrated. This is a significant observation since the method of calculating $\overline{P}$ at multiple T_0 may be used to estimate the equilibration temperature of a sample, as discussed below.

In response to problem 3), we investigated the model reaction Mg_2SiO_4 (fo) + $Fe_2Si_2O_6$ (cfs) = Fe_2SiO_4 (fa) + $Mg_2Si_2O_6$ (cenh), which is not included explicitly among our reactions, but appears implicitly since it is obtained by subtracting r2 from r1. Taking both our own database and that of Loucks (1996), we recalibrated the clinopyroxene and olivine models, treating fo + cfs = fa + cenh as a single-reaction thermometer. The key changes made to the clinopyroxene model through this approach were to $\Delta G_{\mathrm{cen}}^{\mathrm{tran}}(P,T)$ and $\Delta G_{\mathrm{cfs}}^{\mathrm{tran}}(P,T)$, which were recalibrated while preserving their fit to the estimated transition curves in P—T space (taken from Boyd et al. 1964, as interpreted by Gasparik 1990, for enstatite-clinoenstatite; and from Lindsley 1981, for ferrosilite-clinoferrosilite). We also decreased the value of $\Delta G_{\mathrm{fmc}}^{\mathrm{od}}(P,T)$ from −4.4 kJ mol^{-1} to −6.5 kJ mol^{-1}. Minor adjustments were made to the relatively well-known interaction energies in the CaO—FeO—MgO—SiO_2 system, $W_{(\mathrm{di,cfs})}$, $W_{(\mathrm{di,fmc})}$, $W_{(\mathrm{cenh,cfs})}$, and $W_{(\mathrm{cfs,fmc})}$, while respecting the experimental constraints placed on them (Turnock and Lindsley 1981; Lindsley 1983; see Green et al. 2016). The revised values are considered to be better constrained than the originals. The modified models continue to predict temperatures for the fo + cfs = fa + cenh reaction with a large scatter, but now with a reasonable standard error of estimate of ±71ºC.

We made further adjustments to many of the less well-constrained interaction energies, with reference to both the fo + cfs = fa + cenh reaction and the results of avP calculations on the experimental database. These adjustments involved reducing the size of the interaction energies by ~40%. In modifying the interaction energies, we treated them as falling into groups that should retain similar values: (1) the W([cenh,cfs,fmc],[jd,acm]) parameters (notation indicates interaction energies between each of the end-members in the first square brackets with each of the end-members in the second); (2) the W([cenh,cfs,fmc],[cats]) parameters; (3) the W([jd,acm],[cats]) parameters. W([di],[cats]) was adjusted independently. These modifications greatly reduced the excessive avP estimates for COlP (Fig. 5b), and removed the high residuals associated with a_{cats} and a_{jd} when SCOlP is used. Furthermore, values of σ_{fit} for the experiments typically decreased, with fewer experiments

failing the χ^2 test; this was a valuable indication that the adjustments tended to make the models, as a set, predict a more mutually consistent set of independent reactions given the experimental phase compositions.

Individual changes made to the poorly-constrained interaction energies should not necessarily be regarded as improvements to the original *a—x* relations, since avP in general demands less accurate *a-x* relations than the forward-modelling calculations for which the Green et al. (2016) clinopyroxene model was developed. However it is interesting that a much less non-ideal model was required to produce good avP results, especially considering that the pressure information in reactions r1-r3 is related primarily to formation of aluminous pyroxene from plagioclase (i.e. Ca-tschermak + Quartz = Anorthite). The thermodynamics of the key pyroxene and plagioclase end-members in the Holland and Powell (2011) dataset, including the crucial volumetric parameters, are expected to be well known.

Olivine. We initially followed Jennings and Holland (2015) in adopting a simple symmetric model for a forsterite—fayalite solid solution, with Mg—Fe mixing on two identical M sites, as per Hackler and Wood (1989), with W(fo,fa) = 8 kJ mol^{-1}. During refitting of the reaction fo + cfs = fa + cenh, we found it necessary to introduce order-disorder, via an ordered end-member $Fe^{M1}Mg^{M2}SiO_4$ (olfm; compare with discussion of ordered end-member fmc above; see also Supplementary Materials 3), with a Gibbs energy function given by $G_{\rm olfm}(P,T) = ½ \{(G_{\rm fo}(P,T) + G_{\rm fa}(P,T)\} + \Delta G^{\rm od}_{\rm olfm}(P,T)$, and $\Delta G^{\rm od}_{\rm olfm}(P,T) = (-8 + 0.003\ T + 0.02\ P)$ kJ mol^{-1}. This expression yields −3.8 kJ mol^{-1} at 1100ºC and 5 kbar, and remains negative, i.e. favouring ordering, below 2300ºC within the pressure range of interest. $\Delta G^{\rm od}_{\rm olfm}(P,T)$ is thus of a physically plausible size over the *P-T* range of interest, comparable with $\Delta G^{\rm od}_{\rm fmc}(P,T)$. We stress, however, that our calibration does not provide unique constraints on the *a*, *b* and *c* terms of $\Delta G^{\rm od}_{\rm olfm}(P,T)$ and they should be considered essentially as fit parameters, compensating for other difficulties in modelling Fe-Mg exchange between olivine and clinopyroxene in natural systems.

Spinel. Jennings and Holland (2015) used the spinel *a—x* relations of Bryndzia and Wood (1990), in the system MgO—FeO—Fe_2O_3—Al_2O_3—Cr_2O_3, in which all cations mix on three identical sites. Such a model greatly simplifies the mixing behaviour of spinel, by neglecting cation and magnetic disordering. Nevertheless, Bryndzia and Wood (1990) applied it successfully to oxy-barometry of spinel peridotites, and it performed convincingly in the forward calculations of Jennings and Holland (2015), also on peridotite. Therefore we initially adopted the Bryndzia and Wood (1990) *a—x* relations, extended to include TiO_2 by T.J.B. Holland (personal communication; see Supplementary Material 3).

For the majority of experiments that contained magnetite rather than Cr/Al-spinel, we found that avP calculations with SCOlP had a tendency to underestimate experimental pressures, even when calculations with COlP tended to overestimate them. Modifications to the clinopyroxene model, as described above, reduced $\overline{P}$ estimates for both assemblages. To overcome this discrepancy between the assemblages, and following the observation that the end-members sp and herc showed large uncertainty-normalised residuals in activity (as suggested by the avP diagnostics), we were obliged to add large $\Delta G_i^{mod}(P,T)$ terms, of 5 kJ mol^{-1}, to the sp and herc end-members. These terms may be crudely compensating for the highly simplified form of the spinel *a—x* relations, and indeed any unidentified weaknesses elsewhere in the set of thermodynamic models, that compensate for each other in COlP. Additionally, we found that pressures for experiments containing Cr/Al-spinel were routinely overestimated. We were able to prevent this by adjusting the value of $W_{sp\text{-}picr}$ from 39 to 23 kJ mol^{-1}, and that of $W_{herc\text{-}picr}$ from 27 to 16 kJ mol^{-1}. The modifications also allowed most of the experiments to pass the χ^2 test, whereas, using the original spinel model, most of SCOlP calculations failed, with $\sigma_{fit} >> 1.49$.

Inputs for avP: compositions, uncertainties, P_0 and T_0

Mineral formulae for the SCOlP/COlP phases in the experimental runs and natural samples were recalculated from the compositions determined by electron microprobe. Iron was assumed to be all

ferrous in olivine and all ferric in plagioclase. Fe^{3+} in clinopyroxene and spinel was calculated from stoichiometry following the method of Droop (1987). Mineral formulae were then converted into compositional variables suitable for the *a—x* relations (Supplementary Material 2). THERMOCALC (Powell and Holland 1988) version 3.47i was used to run the avP algorithm on these data, generating a value of $\overline{P}$ based on each assemblage for each experiment. The results obtained from the avP algorithm are sensitive to the relative size of uncertainties specified for the compositional variables, and also to those applied to the interaction energies, $W_{(m,n)}$, in the *a—x* relations.

Since rigorous error propagation is not applicable to our experimental database (see Supplementary Material 4), uncertainties on most of the compositional variables for the experimental samples have been simply set to ± 0.01 apfu, a default value typically adopted in avP (Powell and Holland 2008). Given the difficulty of quantifying realistic uncertainties on the spinel *a–x* model, which does not account for cation ordering, uncertainties on x^{sp} $[Fe^{2+}/(Fe^{2+}+Mg)]$ and f^{sp} $[Fe^{3+}]$ have been set to 0.04 apfu, with the aim of accounting for the possible oversimplification of spinel *a-x* relations. This simplified set of compositional uncertainties was then compared with the true uncertainties, derived from partial error propagation, during trial calculations on the refined experimental database using SCOlP equilibria. No significant difference was found in the results. In this test, we also noted that the maximum variations of $\overline{P}$ between different uncertainties assumptions are on the order of $\sigma_{\overline{P}}$, as suggested by Powell and Holland (2008).

For the natural samples, the mineral compositions used for thermobarometry are taken from individual spot analyses of adjacent crystal rims, since adjacent rims are assumed to most closely represent the equilibrium assemblage. The compositional errors are initially derived from counting statistics of the electron microprobe (Supplementary Table 5). Given that such errors are small and weakly correlated, partial error propagation is assumed to yield sufficiently realistic uncertainties for most of the *a–x* model compositional variables. However, after applying the partial error, uncertainties

406 on compositional variables x(sp) and f(sp) (Supplementary Material 2) have been increased by a factor
407 of 4, consistent with the modifications adopted for the experimental samples described above.

408 By default in THERMOCALC, uncertainties on the interaction energies are set to ± 2 kJ mol^{-1} (Powell
409 and Holland 2008). For the *a–x* models used here, uncertainties on many interaction energies are not
410 well constrained and therefore we chose initially to retain this approximation during the assessment of
411 avP calculations on the experimental database. Once the final set of modified *a–x* models had been
412 selected, we noted that avP calculations produced low σ_{fit} (<< 1.0) for many experimental runs and
413 natural samples, implying that the overall input uncertainties were in many cases excessive. We
414 therefore reduced the uncertainties on interaction energies to ± 1 kJ mol^{-1}, which increased to σ_{fit} values
415 generally closer to 1.0 (Supplementary Material 1 and Table 3) and decreased $\sigma_{\bar{P}}$ by about 0.2 kbar.
416 Such generalised uncertainties on interaction energies were adopted as they represent the best
417 compromise to simultaneously obtain low $\sigma_{\bar{P}}$ and successfully prediction of experimental pressures. In
418 fact, this might be a realistic estimate of the uncertainties on the most critical parameters, but many of
419 the less influential parameters are much less well known.

420 During avP calculations applied to experimental samples, the values of P_0 and T_0 were set to T_{exp}
421 and P_{exp} (we note that uncertainties in the measured pressure and temperature of the experimental runs
422 can be as high as ±0.5 kbar and ±20˚C). In the case of natural samples, P_0 was set to 4 kbar,
423 representing the middle of the range of crustal pressure. For both experimental and natural samples, the
424 window within which the avP algorithm should search for the P_r values was set to P_0 ± 20 kbar.
425 Methods for choosing T_0 for natural samples are discussed in a later section.

426 **AvP calculations on the experimental database**

427 In this section we report the results of avP calculations on the experimental database using the refined
428 thermodynamic models and the associated uncertainties adopted in this work.

AvP output: $\overline{P}$, $\sigma_{\overline{P}}$ and σ_{fit}

Spinel + clinopyroxene + olivine + plagioclase equilibria (SCOlP). The results of calculations using SCOlP on the 62 experimental samples are good, as shown in Figure 5a (see also Supplementary Material 1). 65% of the calculations passed the χ^2 test (i.e., $\sigma_{fit} < 1.49$), which indicates that the experimental mineral compositions and the thermodynamic data, with their associated uncertainties, can be safely combined in the averaging procedure. Slightly higher σ_{fit} values (no more than 20% higher than the cut-off imposed by the χ^2 test) might still be considered acceptable, especially since $\sigma_{\overline{P}}$ is increased by a factor equal to σ_{fit} when the χ^2 test is failed. This would increase the proportion of acceptable calculations to 82%. For the calculations that passed the χ^2 test, $\sigma_{\overline{P}}$ varies between 0.80 and 2.10 kbar, with a mean value of 1.24 kbar. Considering all the calculations, the experimental pressures are predicted within $\sigma_{\overline{P}}$ for 67% of the samples, consistent with the expectation that the interval $\overline{P} \pm \sigma_{\overline{P}}$ will encompass the experimental pressure 68% of the time. The accuracy of avP can also be demonstrated by calculating SEE for $\overline{P}$. For the selected experimental dataset the calculated $\overline{P}$ yields a SEE of ± 1.37 kbar (± 1.20 kbar considering only calculations with χ^2 test passed), which is small relative to the typical values obtained by the existing geobarometers for gabbroic assemblages. For example, the clinopyroxene-orthopyroxene barometer of Putirka (2008) (his eq. 39) has SEE = ± 2.8 kbar using his experimental database and SEE = ± 2.7 kbar using our filtered experimental database (see Supplementary Material 1) in the P range 0.5–10 kbar.

No dependence of the pressure residuals ΔP ($\overline{P} - P_{exp}$) on P_{exp} (Fig. 5a) or T_{exp} (Fig. 6a) is observed, suggesting that the *P*- and *T*-dependency of the adopted *a–x* relations is appropriate for the purpose of avP calculations. Furthermore, the residuals are not dependent on the composition of plagioclase (An = 25–94 mol %), olivine (Fo = 61–95 mol %) or spinel ($Fe^{3+}/[Fe^{3+}+Al+Cr]$ = 0.00–0.90; Fig. 6b). For clinopyroxene, the residuals do not appear to vary with composition, although a slight dependence of

$\sigma_{\overline{P}}$ with mg# might be inferred (Fig. 6c), given the apparent higher values of $\sigma_{\overline{P}}$ when mg# < 0.80. No correlations or systematic deviations in ΔP are observed between hydrous and nominally-anhydrous experiments (Supplementary Material 1). Overall, the application of avP to SCOlP with the adopted thermodynamic model produces satisfactory results for a wide range of experimental compositions, and can therefore be applied with confidence to natural mafic and ultramafic rocks that contain spinel, clinopyroxene, olivine and plagioclase. More accurate $Fe^{3+}/\Sigma Fe$ estimations for clinopyroxene and spinel would likely increase the accuracy of the calculated pressures. However, the good avP results obtained in our calculations suggest that the errors related to Fe^{3+} calculated from stoichiometry do not generally have a significant deleterious effect on $\overline{P}$.

Clinopyroxene + olivine + plagioclase equilibria (COlP). Fig. 5b shows the results of avP calculations with COlP equilibria on the same experimental dataset used for SCOlP. Most of the calculations passed the χ^2 test ($\sigma_{fit} < 1.73$) and $\sigma_{\overline{P}}$ varies between 0.93 kbar and 3.20 kbar. Results for samples at $P_{exp} \geq 5$ kbar show a good agreement with the experimental pressures and low calculated uncertainties (Fig. 5b). However, pressures are overall predicted within the uncertainties for a smaller proportion of experiments (54%), which is linked to a systematic overestimation of ~ 1.5 kbar for samples equilibrated at $P_{exp} < 5$ kbar. Comparable results were obtained on the entire dataset of 209 experiments containing COlP (Supplementary Material 6). We suspect that the source of the overestimation at lower pressures could be an excess amount of Al^{IV} in clinopyroxene related to growth rate (Mollo et al. 2010), which is expected to have a relatively larger effect where equilibrium values for Al^{IV} are low, i.e., at low pressures. This issue does not significantly influence the accuracy of $\overline{P}$ when reactions involving spinel end-members are included in the independent set (i.e., SCOlP).

AvP output: residuals and correlations

In this section we examine the results of the least-squares minimization for the individual end-members involved in the reactions and the correlation between the six SCOlP reactions. The low σ_{fit} values obtained for most of the calculations on the experimental database indicate that, in general, the calculated end-member activities and enthalpies do not have to be adjusted outside their uncertainties to obtain a consistent value of P (i.e. $\overline{P}$) for the six reactions. In the avP diagnostics this is shown by the low uncertainty-normalised residuals in log (activity) (e_i^*) and the enthalpy (H_i^*) for each end-member i (see Supplementary Material 2). For calculations that passed the χ^2 test, $|e_i^*|$ is always <2.5 and $|H_i^*|$ is always <1.0 for all end-members. No systematic outliers appear for the calculations on different samples, with both e_i^* and H_i^* scattering randomly around zero. The only exception is for the end-member acmite, which shows e_i^* varying between -0.1 and 2.5 and H_i^* between -0.2 and 1.4. Possibly, such systematic positive residuals indicate a slight systematic overestimation of Fe^{3+} in clinopyroxene as determined by stoichiometry. For calculations that did not pass the χ^2 test no end-member is identifiable that systematically shows high residuals (i.e., $|e_i^*| > 2.5$ and $|H_i^*| > 1.0$). The diagnostic h_i (see Supplementary Material 2) shows that for most of the experimental samples no single end-member has a prevailing influence on the calculated $\overline{P}$. The end-members that are most likely to be influential are cats, cenh, sp, herc and jd. However, in a typical calculation such as that illustrated in the Supplementary Material 2, if the uncertainty on $\ln a_i$ of any single end-member i is doubled, the value of $\overline{P}$ changes by ≤ 0.2 kbar, except in the case of cats for which it is reduced by 0.4 kbar.

Supplementary Material 7 shows the correlation matrixes of the enthalpies of reactions (ΔH_r), $\ln K_r$ and P_r, for the calculations on the experimental database. The matrix of ΔH_r values is the same in each calculation. ΔH_r values for the reaction pairs r1-r4 (0.729), r2-r4 (0.746) and r3-r5 (0.741) are particularly highly correlated due to their shared end-members. These reaction pairs also show relatively highly correlated values of $\ln K_r$, but the magnitude of the correlations in $\ln K_r$, and consequently in P_r, are strongly dependent on phase compositions. In a calculation for which P_{r3} and P_{r5}

have a correlation coefficient of 0.99, these two reactions amount to a single independent constraint on how the end-member properties should be adjusted to attain a consistent $\overline{P}$. However, in calculations involving other phase compositions these reactions show only weak to moderate correlation.

Sensitivity of AvP to P_0 and T_0

Calculations with avP require an initial estimate of pressure (P_0) and temperature (T_0) to be specified. These are needed for the initial calculation of end-member enthalpies and activities. We performed a test to investigate how different assumptions about P_0 and T_0 may influence the calculated SCOlP equilibria and the subsequent results of avP. Multiple calculations with avP on the selected experiments have been performed, firstly varying P_0 in the range 0–15 kbar (with $T_0 = T_{exp}$) and then varying T_0 in the range 600–1400˚C (with $P_0 = P_{exp}$). The first tests showed a negligible effect of P_0 on the calculated pressure. For the sample ShR658 (P_{exp} = 2.0 kbar, T_{exp} = 1075 ˚C; Supplementary Material 1), for example, a substantial difference of 15 kbar in P_0 produces a difference in the calculated $\overline{P}$ of 0.01 kbar ($\overline{P}$ = 2.94 ± 1.62 kbar if P_0 = 0 kbar; $\overline{P}$ = 2.95 ± 1.62 kbar if P_0 = 15 kbar), with no difference in the quality of the fit. Similar results have been observed for other experimental samples in the dataset.

On the other hand, different assumptions about T_0 variably affect the calculated $\overline{P}$. An example is reported in Fig. 7, which shows the results for the same experiment ShR658. In this case, the temperature dependence of $\overline{P}$, $d\overline{P}/dT_0$, corresponds to -0.012 kbar/˚C. More generally the test on the experimental dataset showed that $d\overline{P}/dT_0$ is always negative. Furthermore, the absolute value of the dependence of $\overline{P}$ on T_0 is smaller for greater values of $\overline{P}$, with $d\overline{P}/dT_0$ varying from -0.016 to -0.002 kbar/˚C (Fig. 8). This indicates that, for natural assemblages equilibrated at high pressures, even errors related to crude temperature estimates (e.g., from geological/petrological inferences) will not significantly increase the uncertainty on the calculated pressure (i.e., additional ± 0.4–0.6 kbar for errors on T_0 on the order ± 150–200˚C).

For assemblages equilibrated at relatively low pressures (<5kbar), uncertainties on T_0 on the order of 150–200˚C might increase the total pressure uncertainties by 1.5–2.5 kbar, which indicates the need of reliable methods to estimate equilibration temperature when applying avP to natural samples. One such a method is to carry out the avP procedure at multiple temperatures, and observe the variation in the value of σ_{fit}. If the variation of σ_{fit} with T_0 follows a polynomial function of the type $\sigma_{fit} = a'T_0^2 + b'T_0 + c'$ (where a', b' and c' are constants and a' > 0, b' < 0), and a minimum of σ_{fit} is clearly identifiable (e.g., Fig. 7), then the value of T_0 that gives the minimum value of σ_{fit} can be considered to give better estimates of T. Figure 7 shows a successful example of such a method, in which the estimated temperature ($T\sigma_{fit}$; 1050˚C) is close to the measured experimental temperature, T_{exp} (1075˚C). We applied such a method to the selected experimental dataset, firstly to evaluate the reliability of the estimated temperatures and secondly to assess how the possible errors associated with these estimates affect the calculated $\overline{P}$. For some experiments the variation of σ_{fit} with T_0 is such that a minimum in σ_{fit} cannot be identified and therefore these experiments (n = 25) have been removed from the test dataset. The results of the test are reported in Figure 9, which shows that $T\sigma_{fit}$ predicts the experimental temperatures with a SEE of ± 93˚C (n = 37). Application of avP to the same experimental dataset, adopting $T_0 = T\sigma_{fit}$ instead of $T_0 = T_{exp}$, still produces acceptable calculated pressures (cf. Figs. 9b and d).

We note that $\sigma_{\overline{P}}$ also varies with T_0, and the minima in $\sigma_{\overline{P}}$ and σ_{fit} do not generally occur at the same T_0. This suggests that temperature is not strongly constrained in the sample. We find empirically that the optimal T_0 is usually better predicted by the minimum in σ_{fit}, even when σ_{fit} passes the χ^2 test over a wide range of temperatures. The use of $T_{\sigma_{fit}}$ as a possible T estimate can be justified in that σ_{fit} characterises the compatibility of the different independent reactions, and T_0 contributes to the formulation of those reactions without being formally included in the covariance matrix summarised by $\sigma_{\overline{P}}$.

In conclusion, P_0 does not have significant effects on the calculated $\overline{P}$ at any condition and therefore we suggest the initial estimate to be always set to 4 kbar (i.e., mid-crustal values). On the other hand, the effect of T_0 might be in some cases significant, but it can be easily evaluated for each sample by running multiple avP calculations at different T_0. If no other thermometer can be applied that gives T uncertainties < 90 ºC, then $T_0 = T_{\sigma_{\text{fit}}}$ can be used to produce the best estimate of P.

Application to natural rocks

Given the success of tests on the experimental dataset, we next applied the refined thermodynamic models to estimating the pressure of formation of igneous rocks, choosing samples containing spinel, clinopyroxene, olivine and plagioclase. We carefully selected two groups of mafic/ultramafic xenoliths with texture, mineralogy and mineral chemistry suggesting good attainment of chemical equilibrium. Compositions of minerals in these natural samples are reported in Fig. 2. The first group of xenoliths, from the island of Dominica, Lesser Antilles, provides an example of the application of avP to gabbroic rocks from a mid-upper island arc crust. The second group, which was described and analysed by McGuire (1994) and McGuire and Mukasa (1997), is from the Wikieup volcanic field, Arizona, and provides an example of gabbroic and ultramafic xenoliths from the lower continental crust. Unless otherwise specified, the following discussion refers to calculations with SCOlP.

Gabbroic xenoliths from Dominica, Lesser Antilles

Background, sample description and analyses. The Lesser Antilles is an active volcanic arc resulting from westwards subduction of the South American plate beneath the Caribbean plate (Macdonald et al. 2000). The volcanic products, which vary from basalts to andesites and dacites, host a large number of plutonic xenoliths showing a variety of mineralogical compositions (Arculus and Wills 1980; Tollan et al. 2012; Stamper et al. 2014b; Cooper et al. 2016). The ubiquity of these xenoliths provides an exceptional opportunity to investigate the nature of the crust and the evolution of magmatic systems in

an island arc setting, but such an investigation requires precise estimates of the pressure of formation of the xenoliths. Given that the estimated thickness of the crust in the Lesser Antilles varies between 25 and 35 km (cf., Boynton et al. 1979; Christeson et al. 2008; Kopp et al. 2011), the gabbroic xenoliths are likely to have equilibrated at pressures between ~1 and ~8 kbar. Therefore, only geobarometric estimates with low associated uncertainties (<2 kbar) can provide useful insight into the vertical distribution of mafic lithologies in the crust.

Dominica, in the centre of the arc, is mainly composed of Pliocene to recent volcanic rocks (Lindsay et al. 2005; Howe et al. 2015). Plutonic xenoliths, mostly consisting of gabbroic assemblages with or without olivine, orthopyroxene and hornblende, have been found as clasts in young, reworked sediments from the southern part of the island. For the purpose of testing the applicability of the avP method, we selected three xenoliths containing the assemblage SCOlP, which have been collected from marine deposits close to the village of Petite Savanne (southern Dominica), on the edge of the Foundland volcanic centre. A schematic description of these samples, highlighting the main textural and mineralogical features, is shown in Supplementary Material 8. Note that xenolith DC93 is composed of two parts (a coarse-grained troctolite, DC93a, attached to a heterogranular Ol-gabbronorite, DC93b).

Details of electron microprobe analyses and results are reported in the Supplementary Material 5. Compositions of olivine, spinel, clinopyroxene and plagioclase (Fig. 2) are similar to those found in other cumulate xenoliths from the Lesser Antilles (e.g., Tollan et al. 2012; Stamper et al. 2014b; Cooper et al. 2016). Coexisting olivine and plagioclase show relatively low forsterite contents (68–73 mol% Fo) and high anorthite contents (87–93 mol% An) respectively; clinopyroxenes are augites showing a limited range of mg# (78–82 %); spinels are titanomagnetites with TiO_2 contents of 7.6 to 9.2 wt%. Grain-to-grain and core-rim variations for olivine, spinel, pyroxenes and plagioclase are small, suggestive of well-equilibrated assemblages. The largest compositional variations are observed

592 in samples DC91 and DC93b (e.g., $Al_2O_3^{cpx}$ = 1.9–3.7 wt% for DC91). Clinopyroxene in DC93b shows
593 a poikilitic texture with anhedral spinel inclusions and a slight patchy zoning mainly limited to Al^{IV}
594 (0.07–0.13 apfu) and Fe^{3+} (0.03–0.04 apfu). For the purpose of thermobarometry, only the
595 compositions of adjacent crystal rims have been used (Fig. 10).

596 **Average P calculations.** Mineral compositions reported in Supplementary Material 5 have been used
597 to calculate $\overline{P}$, adopting the thermodynamic models and calculation methods described above (see also
598 Supplementary Material 2 for the example of an avP calculation on sample DC90). T_0 has been
599 estimated by running a calculation every 10˚C in the range 700–1200˚C, and selecting the temperature
600 that produce the lowest σ_{fit} ($T\sigma_{fit}$) (see above and Fig. 7). Temperatures calculated with this method
601 (870–1000˚C) and results of avP calculations are reported in Table 3. All calculations produced low σ_{fit}
602 values (0.81–1.54) and $\sigma_{\overline{P}}$'s for each sample are low (0.91–1.55 kbar). The lowest $\sigma_{\overline{P}}$ is obtained for
603 the ol-gabbronorite DC90 ($\overline{P}$ = 3.58 ± 0.91 kbar), which is the sample with the smallest compositional
604 heterogeneities and best-equilibrated texture (e.g. ~120˚ grain boundaries). The cpx-amph-gabbronorite
605 DC91 contains also minor orthopyroxene, which allowed for application of cpx-opx thermometry
606 (Putirka 2008; Table 3). T estimated with this method is in agreement with $T\sigma_{fit}$ (896 vs 910 ˚C),
607 although the observed $K_D(Fe\text{-}Mg)^{cpx\text{-}opx}$ is below the range considered by Putirka (2008) to demonstrate
608 equilibrium (i.e., 0.79 vs. 1.09 ± 0.14). Pressure estimated for this sample (at $T_0 = T\sigma_{fit}$) is 1.94 ± 1.09
609 kbar. For all four Dominica samples, uncertainty-normalised residuals are low ($|e_i^*| < 1.5$, $|H_i^*| < 0.27$),
610 with acmite showing somewhat higher values (($|e_{acm}^*| < 2.1$, $|H_{acm}^*| < 0.87$), as observed for the
611 calculations on the experimental database. End-members cats, cenh, and jd show the highest, but still
612 acceptable, h_i values (h_{cats} = 0.26–0.30, h_{cenh} = 0.12–0.18, h_{jd} = 0.29–0.35). Calculations with COlP
613 produced comparable pressure estimates and uncertainties, although $\overline{P}$ is systematically higher (by ≤ 1
614 kbar, Table 3), as previously observed in tests on the experimental database at P_{exp} < 5 kbar.

615 The composite xenolith DC93 contains two assemblages (DC93a, DC93b; Supplementary Material
616 8 and Fig. 10) that show different textures and degrees of chemical and textural equilibrium despite
617 likely forming at the same pressure. Ol-gabbronorite DC93b show somewhat larger compositional
618 heterogeneities and lower Al^{IV} and Fe^{3+} in clinopyroxene compared to troctolite DC93a
619 (Supplementary Material 5), which is most likely related to a difference in bulk composition. This
620 provides an opportunity to test the effect of such heterogeneities on avP calculations with SCOlP.
621 Calculated pressures for samples DC93a and DC93b are in good agreement (2.67 ± 1.35 kbar vs, 2.81
622 ± 1.55 kbar), supporting the robustness of avP.

623 The geobarometric results obtained for these samples give an estimate of the pressures of magma
624 storage and crystallization in southern Dominica. Overall, the calculated pressures are in agreement
625 with the range inferred by observational and experimental studies on magmas and cumulate rocks from
626 the Lesser Antilles (i.e. mostly 1.0–5.0 kbar for gabbroic assemblages; c.f., Pichavant and Macdonald
627 2007; Stamper et al. 2014b; Melekhova et al. 2015; Cooper et al. 2016). Pressure calculated for the
628 cpx-amph-gabbronorite DC91 (1.94 ± 1.09 kbar) agree very well with the pressures of orthopyroxene
629 and plagioclase crystallization in lavas from southern Dominica (~2 kbar; Gurenko et al. 2006),
630 estimated using melt inclusion data and H_2O-CO_2 solubility models. Considering an average density
631 ($\bar{\rho}$) of the crust of 2800 kg/m^3, the calculated $\overline{P} \pm \sigma_{\overline{P}}$ for this cpx-amph-gabbronorite corresponds to a
632 depth of 7.1 ± 4.0 km, which agrees with the estimated hypocentres of deep volcanic earthquakes in the
633 nearby Plat Pays volcanic complex (2–6 km; Lindsay et al. 2003), thought to result from pressurization
634 of the magma reservoirs. Note that application of the cpx-opx geobarometer of Putirka (2008; his eq.
635 39) to the same sample DC91, which produces an estimated value of 1.6 kbar (as stated above, K_D[Fe-
636 Mg]$^{cpx\text{-}opx}$ < 0.95 potentially flags incomplete equilibration), is accompanied by a model uncertainty of
637 ± 2.8 kbar (Putirka 2008). This corresponds to an uncertainty of ± 10.2 km in the estimated depth of
638 formation.

Pressures estimated for ol-gabbronorite DC90 and troctolite DC93a correspond to depths of 13.0 ± 3.3 km and 9.7 ± 4.9 km respectively. Based on the seismic reflectors identified for the crust north of Dominica (Kopp et al. 2011), such depths correspond to the middle-to-upper crust transition. Figure 11 shows how the thermobarometric results on all three xenoliths compare with the geophysical model of Kopp *et al*. (2011). Note that among the existing geobarometers calibrated for basaltic compositions, only the single-clinopyroxene formulations of Nimis (1995) and Putirka (2008) could be applied to these assemblages[2]. Application of equation 32a of Putirka (2008) produces P = 9.4 ± 3.1 kbar for the sample DC90 and P = 9.9 ± 3.1 kbar for the sample DC93a, which corresponds to depths of 34.2 ± 11.3 km and 36.0 ± 11.3 km, respectively, exceeding the crustal thickness in this area (27 km; Kopp et al. 2011). Overall, the successful application of avP to these samples suggest that future studies on a more extensive xenolith suite from Dominica and elsewhere in the Lesser Antilles arc, combined with petrological and geophysical observations, may help to constrain the lithological structure of the crust with a precision not previously achievable.

Mafic and ultramafic xenoliths from Wikieup, Arizona

Background and sample selection. The Wikieup volcanic field is located in the Arizona Transition Zone (south-western United States), between the Basin and Range Province (BRP), a region of thinned continental crust (20–30 km), and the Colorado Plateau (CP), characterized by a thicker crust (40-50 km) that remained tectonically stable over the Phanerozoic (e.g., Bashir et al. 2011). The Wikieup volcanics host a large number of mafic and ultramafic xenoliths thought to represent portions of the underlying deep crust and upper mantle. Some of the xenoliths analysed by McGuire (1994) and later by McGuire and Mukasa (1997) contain the assemblage SCOlP, making them suitable for application of the avP method. Quantifying the thickness and nature of the crust in the Arizona Transition Zone is important to interpret the tectonic and magmatic events that shaped the lithosphere of the southwestern

[2] Note that there are no tests for equilibrium (e.g., Putirka 2008) for clinopyroxene-only models.

US. Consequently a large number of geophysical investigations have been carried out in this area (e.g., Hauser et al. 1987; Parsons et al. 1992; Bashir et al. 2011 and reference therein), providing a context for our thermobarometric results. McGuire (1994) presented such an approach using gabbroic xenoliths, but due to the lack of reliable geobarometers for such assemblages, the estimated pressures were poorly constrained.

Of the xenoliths described and analysed by McGuire (1994) and McGuire and Mukasa (1997) we used four samples, from Tertiary alkaline olivine-basalts (Wilshire 1990) on the eastern flank of the Hualuapai Mountains, that contain the assemblage SCOlP and for which mineral compositions are available. Samples WK2-9 and WKa-49a are ol-gabbros; samples WK1-24 and WK1-63 are plagioclase-peridotites. The latter show higher plagioclase and lower olivine contents with respect to typical mantle peridotites, but show compositional and textural features that distinguish them from the ol-gabbros (McGuire and Mukasa 1997). Both pl-peridotites and gabbros show allotriomorphic-granular textures but pl-peridotites are also often foliated. Some textural evidence of early-stage reactions between plagioclase and olivine grains has been reported (McGuire and Mukasa 1997), but compositional heterogeneity is limited to some plagioclase grains that show slight normal zoning (< 2% An; McGuire and Mukasa 1997). Phase compositions are shown in Fig. 2 and detailed microprobe analyses are reported in McGuire (1994) and McGuire and Mukasa (1997). Olivine shows a limited variation in composition (Fo_{77-79}); spinel is Al-rich ($Al/[Al+Cr+Fe^{3+}]$ = 0.90–0.97) with low TiO_2 contents (0.11–0.45 wt%); clinopyroxenes are augites with Al_2O_3 contents varying from 6.91 to 7.49 wt%; and plagioclase varies between An_{52-53} (pl-peridotites) and An_{58-71} (ol-gabbros).

AvP calculations. All avP calculations passed the χ^2 test and the calculated uncertainties are notably low (0.95–1.00 kbar; Table 3). Estimated pressures are similar within the uncertainties for all four samples, but ol-gabbros shows some apparent lower values than pl-peridotites (Table 3). Similar estimates are obtained using COlP, with no significant difference in the calculated uncertainties (Table

686 3), as previously observed at P > 5 kbar for our experimental test (cf., Figs. 5a and b). Note that ol-
687 gabbro WK2-9 and pl-peridotite WK1-63 also contain orthopyroxene, allowing $T\sigma_{fit}$ to be compared
688 with the results of cpx-opx thermometry (Putirka, 2008). Observed $K_D(Fe\text{-}Mg)^{cpx\text{-}opx}$ (0.94–0.95) are
689 within the range recommended for the application of such thermometer (Putirka, 2008). Temperatures
690 for the ol-gabbro WK2-9 agree fairly well (940˚C vs. 887˚C), while temperatures for the pl-peridotite
691 WK1-63 disagree by about 200˚C (Table 3). However, calculations for WK1-63 using T_0 estimated
692 from cpx-opx thermometry (T_0 = 953˚C instead of T_0 = 1150˚C) produce relatively small differences in
693 the calculated pressure (7.78 ± 0.86 kbar vs. 6.88 ± 0.97 kbar).

694 When calculated pressures for all four samples are converted to depths (Table 3), the resulting
695 values are consistent with those suggested by McGuire (1994) and McGuire and Mukasa (1997) based
696 on: i) the observation that many composite xenoliths show contact between gabbros and mantle
697 peridotites, suggesting an origin from the crust-mantle boundary (McGuire 1994) and ii) projection of
698 calculated temperatures onto the regional geotherm (100 mW/m^2; McGuire and Mukasa 1997). Our
699 calculations place more robust petrological constraints on the equilibration depths for comparison with
700 recent geophysical investigations (Bashir et al. 2011). Figure 12 shows that the calculated depths for
701 the ol-gabbros and pl-peridotites correspond closely to the lower crust levels in the integrated gravity
702 and seismic model of Bashir *et al.* (2011). Note that the upper-lower crust and crust-mantle boundaries
703 sketched in Fig. 12 should be viewed as transition zones and that the geophysical model has an
704 associated uncertainty, which that is not easily quantifiable (Bashir et al. 2011). The fact that both ol-
705 gabbros and pl-peridotites show comparable depths of formation is in agreement with a model of the
706 lower continental crust characterized by a network of dykes and sills of variably mafic lithologies
707 (McGuire 1994; Parsons et al. 1992), that can be related to the magmatic episodes that brought the
708 xenoliths to the surface. Further application of the avP method to a larger number of xenoliths,

combined with detailed modal analyses and integrated geophysical-petrological models, may help to test this hypothesis.

Implications and final recommendations

Application of avP to experimental phase equilibria and well-equilibrated natural rocks has shown, for the first time, that this method can be used to reliably estimate the pressure of formation for mafic and ultramafic igneous rocks. The least squares minimization procedure in avP makes it possible to exploit the power of internally-consistent thermodynamic datasets and mutually compatible *a—x* relations, taking into account both uncertainties and correlations in end-member properties. It represents an optimal method to deal with the inevitable inaccuracy of thermodynamic models and uncertainties on mineral compositions. We demonstrated that calculations on SCOlP equilibria, using the models refined in this work, yield i) good reproducibility of experimental pressures by avP (P is predicted, within the calculated $\sigma_{\overline{P}}$, for 67% of the experimental database), ii) internal consistency of avP results (i.e., χ^2 test passed) for the majority of phase equilibrium experiments and for the selected well-equilibrated natural assemblages, and iii) low P uncertainties ($\sigma_{\overline{P}}$) as low as 0.9 kbar) for the same assemblages. Pressure estimates with such low uncertainties can help to characterise the key petrological processes and trace the vertical distribution of mafic and ultramafic lithologies in the upper 30–40 km of the lithosphere. Integration with geophysical data for the same areas affords potentially powerful insights into crustal structure.

Modifications of the existing *a–x* models for clinopyroxene (Green et al. 2016) and spinel (Jennings and Holland 2015) were necessary to avoid some observed pressure deviations resulting from initial calculations with SCOlP. At present we believe that the thermodynamic models used in this work are applicable to any gabbroic rock, pyroxenite or peridotite that contains olivine + clinopyroxene + plagioclase in its equilibrium assemblage, regardless of geodynamic setting. This is supported by i) the robustness of a multiple-reaction approach based on an internally consistent thermodynamic dataset

(Holland and Powell 2011) and ii) the successful tests on a database of phase equilibrium experiments that cover a wide range of basaltic and peridotitic compositions (e.g., Figs. 5 and 6), both hydrated and nominally-anhydrous. We believe the method can be applied also to volcanic rocks, for which, however, the selection of equilibrium phase compositions might not be straightforward. Future test cases, in which a detailed textural and chemical characterization of the phenocryst assemblages will be coupled with the application of avP and its fit diagnostics, will help to test this hypothesis.

For equilibrated assemblages including spinel, calculations with SCOlP equilibria are always preferred, since COlP slightly overestimate pressures (by 1–2 kbar) at upper-middle crust conditions ($P < 5$ kbar). Calculations with SCOlP should be possible for a large number of mafic/ultramafic rocks, as spinel is a ubiquitous phase in many natural gabbroic and basaltic rocks, and sometimes coexists with plagioclase in shallow mantle peridotites/pyroxenites. Calculations with COlP, on the other hand, are more likely to be needed for plagioclase-only peridotites/pyroxenites. Importantly, the latter typically form at lower crust and uppermost mantle conditions ($P > 5$ kbar; e.g., Kelemen et al. 2007; Borghini et al. 2011), corresponding to those pressures at which COlP calculations show low uncertainties and are consistent with SCOlP based on tests on experimental (Fig. 5) and natural samples (Table 3).

The reliability of avP calculations on natural samples relies on the attainment of equilibrium in the assemblage. If the assemblage shows slight intra- or inter-grain chemical heterogeneities, care should be taken to select mineral compositions that are likely to be at equilibrium, as shown by the application to the cumulate xenoliths from Dominica (Fig. 10). Secondly, when using our sets of independent reactions (Fig. 4), temperature estimates for the sample need to be well constrained if the assemblage equilibrated at $P < 5$ kbar. In order to estimate the true T of equilibration, it may be possible to use existing thermometers, such as the cpx-opx thermometer of Putirka (2008) or the Ca-in-olivine thermometer of Shejwalkar and Coogan (2013). Otherwise we suggest running avP calculations at

different temperature T_0, and select that which produces the lowest residuals (σ_{fit}) in the avP minimization routine (Fig. 7).

Further work is planned to extend the avP approach to a wider range of phase assemblages. This will entail testing and potential modification of thermodynamic models for orthopyroxene, amphibole and ilmenite, which are also common constituents of mafic and ultramafic igneous rocks in various settings. Using such a set of models, it will be possible to obtain mutually consistent pressure estimates for a wide range of igneous rocks.

Funding

This project was funded by NERC grant NE/K014978/1.

Acknowledgments

We thank Roger Powell for helpful discussions, especially his insight into and debugging of the avP algorithm. Susanne Skora provided many useful suggestions in the original formulation of this project and, together with Richard Arculus and Richard Brooker, assisted in collection of the Dominica xenoliths. John Schumacher and Lena Melekhova are thanked for the useful discussions. Francesco Narduzzi is thanked for the valuable comments on preliminary versions of the manuscript. Silvio Mollo and Alexey Ariskin are thanked for their helpful and constructive reviews, and Renat Almeev for his editorial handling.

References

Almeev, R.R., Holtz, F., Koepke, K., Parat, F., and Botcharnikov R.R. (2007) The effect of H_2O on olivine crystallization in MORB: Experimental calibration at 200 MPa. American Mineralogist, 92, 670–674.

777 Andujar, J., Scaillet, B., Pichavant, M., and Druitt, T. H. (2015) Differentiation conditions of a basaltic
778 magma from Santorini, and its bearing on the production of andesite in arc settings. Journal of
779 Petrology, 56, 765–794.

780 Arculus, R., and Wills, K. (1980) The petrology of igneous blocks and inclusions from the Lesser
781 Antilles island arc. Journal of Petrology, 21, 143–168.

782 Baker, M.B., and Stolper, E.M. (1994) Determining the composition of high-pressure mantle melts
783 using diamond aggregates. Geochimica et Cosmochimica Acta, 58, 2811–2827.

784 Barclay, J., and Carmichael, I. S. E. (2004) A hornblende basalt from Wester Mexico: Water-saturated
785 phase relations constrain a pressure-temperature window of eruptibility. Journal of Petrology, 45,
786 485–506.

787 Bartels, K.S., Kinzler, R.J., and Grove, T.L. (1991) High pressure phase relations of primitive high-
788 alumina basalts from Medicine Lake volcano, northern California. Contributions to Mineralogy and
789 Petrology, 108, 253–270.

790 Bashir, L., Gao, S.S., Liu, K.H., and Mickus, K. (2011) Crustal structure and evolution beneath the
791 Colorado Plateau and the southern Basin and Range Province: Results from receiver function and
792 gravity studies. Geochemistry Geophysics Geosystems 12, doi: 10.1029/2011GC003563.

793 Berman, R.G. (1988) Internally-consistent thermodynamic data for minerals in the system Na_2O-K_2O-
794 CaO-MgO-FeO-Fe_2O_3- Al_2O_3-SiO_2-TiO_2-H_2O-CO_2. Journal of Petrology, 29, 445–522.

795 Berman, R.G. (1991) Thermobarometry using multi-equilibrium calculations: a new technique with
796 petrological applications. Canadian Mineralogist, 29, 833–855.

797 Blatter, D.L., Sisson, T.W., and Hankins, W.B. (2013) Crystallization of oxidized, moderately hydrous
798 arc basalt at mid- to lower-crustal pressures: implications for andesite genesis. Contributions to
799 Mineralogy and Petrology, 166, 861–886.

Borghini, G., Fumagalli, P., and Rampone, E. (2010) The stability of plagioclase in the upper mantle: subsolidus experiments on fertile and depleted lherzolite. Journal of Petrology, 51, 229–254.

Borghini, G., Fumagalli, P., and Rampone, E. (2011) The geobarometric significance of plagioclase in mantle peridotites: a link between nature and experiments. Lithos, 126, 42–53.

Boyd, F.R., England, J.L., and Davis, B.T.C. (1964). Effect of pressure on the melting and polymorphism on enstatite, $MgSiO_3$. Journal of Geophysical Research, 69, 2101–2109.

Boynton, C.H., Westbrook, G.K., Bott, M.H.P., and Long, R.E. (1979) A seismic refraction investigation of crustal structure beneath the Lesser Antilles island arc. Geophysical Journal International, 58, 371–393.

Bryndzia, L.T., and Wood, B. J. (1990) Oxygen thermobarometry of abyssal spinel peridotites: the redox state and C–O–H volatile composition of the Earth's sub-oceanic upper mantle. American Journal of Science, 290, 1093–1116.

Chalot-Prat, F., Falloon, T.J., Green, D.H., and Hibberson, W.O. (2010) An experimental study of liquid compositions in equilibrium with plagioclase + spinel lherzolite at low pressures (0.75 GPa). Journal of Petrology, 51, 2349–2376.

Chalot-Prat, F., Falloon, T.J., Green, D.H., and Hibberson, W.O. (2013) Melting of plagioclase + spinel lherzolite at low pressures (0.5 GPa): An experimental approach to the evolution of basaltic melt during mantle refertilisation at shallow depths. Lithos, 172–173, 61–80.

Christeson, G.L., Mann, P., Escalona, A., and Aitken, T.J. (2008) Crustal structure of the Caribbean–northeastern South America arc–continent collision zone. Journal of Geophysical Research, 113, B08104, doi:10.1029/2007JB005373.

Cooper, G.F., Davidson, J.P., and Blundy J.D. (2016) Plutonic xenoliths from Martinique, Lesser Antilles: evidence for open system processes and reactive melt flow in island arc crust. Contributions to Mineralogy and Petrology, 171, 87.

Di Carlo, I., Pichavant, M., Rotolo, S., and Scaillet, B. (2006) Experimental crystallization of a high-K arc basalt: The Golden Pumice, Stromboli Volcano (Italy). Journal of Petrology, 47, 1317–1343.

Diener, J.F.A., Powell, R., White, R.W., and Holland, T.J.B. (2007) A new thermodynamic model for clino- and orthoamphiboles in the system Na_2O-CaO-FeO-MgO-Al_2O_3-SiO_2- H_2O-O. Journal of Metamorphic Geology, 25, 631–656.

Draper, D.S., and Johnston, A.D. (1992) Anhydrous PT phase relations of an Aleutian high-MgO basalt: an investigation of the role of olivine–liquid reaction in the generation of arc high-alumina basalts. Contributions to Mineralogy and Petrology, 112, 501–519.

Droop, G.T.R. (1987) A general equation for estimation of Fe^{3+} concentrations in ferromagnesian silicates and oxides from microprobe analysis, using stoichiometry criteria. Mineralogical Magazine, 51, 431–435.

Erdman, S., Martel, C., Pichavant, M., and Kushnir, A. (2014) Amphibole as an archivist of magmatic crystallization conditions: problems, potential, and implications for inferring magma storage prior to the paroxysmal 2010 eruption of Mount Merapi, Indonesia. Contributions to Mineralogy and Petrology, 167, 1016.

Falloon, T.J., Danyushevsky, L.V., Ariskin, A., Green, D.H. and Fors, C.E. (2007) The application of olivine geothermometry to infer crystallization temperatures of parental liquids: Implications for the temperature of MORB magmas. Chemical Geology, 241, 207–233.

842 Feig, S.T., Koepke, J., and Snow, J.E. (2006) Effect of water on tholeiitic basalt phase equilibria: an
843 experimental study under oxidizing conditions. Contributions to Mineralogy and Petrology, 152,
844 611–638.

845 Feig, S.T., Koepke, J., and Snow, J. E. (2010) Effect of oxygen fugacity and water on phase equilibria
846 of a hydrous tholeiitic basalt. Contributions to Mineralogy and Petrology, 160, 551–568.

847 Fumagalli, P., Borghini, G., Rampone, E. and Poli, S. (2017) Experimental calibration of Forsterite–
848 Anorthite–Ca-Tschermak–Enstatite (FACE) geobarometer for mantle peridotites. Contributions to
849 Mineralogy and Petrology, 172, 38.

850 Gasparik, T. (1990) A thermodynamic model for the enstatite-diopside join. American Mineralogist,
851 75, 1080–1091.

852 Ghiorso, M.S., and Evans, B.W. (2008) Thermodynamics of rhombohedral oxide solid solutions and a
853 revision of the Fe-Ti two-oxide geothermometer and oxygen-barometer. American Journal of
854 Science, 308, 957–1039.

855 Ghiorso, M.S., and Sack, R.O. (1995) Chemical mass transfer in magmatic processes, IV, A revised
856 and internally consistent thermodynamic model for the interpolation and extrapolation of liquid-
857 solid equilibria in magmatic systems at elevated temperatures and pressures. Contributions to
858 Mineralogy and Petrology, 119, 197–212.

859 Giaramita, M., and Day, H. (1990) Error propagation in calculations of structural formulas. American
860 Mineralogist, 75, 170–182.

861 Gordon, T.M. (1992) Generalized thermobarometry: solution of the inverse chemical equilibrium
862 problem using data for individual species. Geochimica et Cosmochimica Acta, 56, 1793–1800.

Green, E.C.R., Holland, T.J.B., and Powell, R. (2007) An order- disorder model for omphacitic pyroxenes in the system jadeite- diopside-hedenbergite-acmite, with applications to eclogitic rocks. American Mineralogist, 92, 1181–1189.

Green, E.C.R., Holland, T.J.B., Powell, R., and White, R.W. (2012) Garnet and spinel lherzolite assemblages in $MgO–Al_2O_3–SiO_2$ and $CaO–MgO–Al_2O_3–SiO_2$: thermodynamic models and an experimental conflict. Journal of Metamorphic Geology, 30, 561–577.

Green, E.C.R., White, R.W., Diener, J.F.A., Powell, R., Holland, T.J.B., and Palin, R.M. (2016). Activity–composition relations for the calculation of partial melting equilibria in metabasic rocks. Journal of Metamorphic Geology, 34, 845–869.

Grove, T.L., and Bryan, W.B. (1983) Fractionation of pyroxene-pyric MORB at low pressure: An experimental study. Contributions to Mineralogy and Petrology, 84, 293–309.

Grove, T.L., and Juster, T. C. (1989) Experimental investigations of low-Ca pyroxene stability and olivine – pyroxene – liquid equilibria at 1-atm in natural basaltic and andesitic liquids. Contributions to Mineralogy and Petrology, 103, 287–305.

Grove, T.L., Donnelly-Nolan, J.M., and Housh, T. (1997) Magmatic processes that generated the rhyolite of Glass Mountain, Medicine Lake volcano, N. California. Contributions to Mineralogy and Petrology, 127, 205–223.

Grove, T.L., Elkins-Tanton, L.T., Parman, S.W., Chatterjee, N., Muntener, O., and Gaetani, G. A. (2003) Fractional crystallization and mantle-melting controls on calc-alkaline differentiation trends. Contributions to Mineralogy and Petrology, 145, 515–533.

Gualda, G.A.R., Ghiorso, M.S., Lemons, R.V., and Carley, T.L. (2012) Rhyolite-MELTS: a modified calibration of MELTS optimized for silica-rich, fluid-bearing magmatic systems. Journal of Petrology, 53, 875–890.

886 Gurenko, A.A., Trumbull, R.B., Thomas, R., and Lindsay, J.L. (2006) A melt inclusion record of
887 volatiles, trace elements and Li – B isotope variations in a single magma system from the Plat Pays
888 Volcanic Complex, Dominica, Lesser Antilles. Journal of Petrology, 46, 2495–2526.

889 Hackler, R.T., and Wood, B.J. (1989) Experimental determination of Fe and Mg exchange between
890 garnet and olivine and estimation of Fe–Mg mixing properties in garnet. American Mineralogist, 74,
891 994–999.

892 Hamada, M., and Fuji, T. (2008) Experimental constraints on the effects of pressure and H_2O on the
893 fractional crystallization of high-Mg island arc basalt. Contributions to Mineralogy and Petrology,
894 155, 767–790.

895 Hauser, C., Gephart, J., Latham, T., Oliver, J., Kaufman, S., Brown, L., and Lucchitta, I. (1987)
896 COCORP Arizona transect: Strong crustal reflections and offset Moho beneath the transition zone.
897 Geology, 15, 1103–1106.

898 Holland, T.J.B., and Powell, R. (1985) An internally consistent thermodynamic dataset with
899 uncertainties and correlations. II. Data and results. Journal of Metamorphic Geology, 3, 343–370.

900 Holland, T.J.B., and Powell, R. (1990) An internally consistent thermodynamic dataset with
901 uncertainties and correlations: The system Na_2O-K_2O-CaO-MgO-MnO-FeO-Fe_2O_3-Al_2O_3-SiO_2-
902 TiO_2-C-H_2-O_2. Journal of Metamorphic Geology, 8, 89–124.

903 Holland, T., and Blundy, J. (1994) Non-ideal interactions in calcic amphiboles and their bearing on
904 amphibole-plagioclase thermometry. Contributions to Mineralogy and Petrology, 116, 433–447.

905 Holland, T.J.B., and Powell, R. (1998) An internally-consistent thermodynamic dataset for phases of
906 petrological interest. Journal of Metamorphic Geology, 16, 309–344.

907 Holland, T.J.B., and Powell, R. (2003) Activity–composition relations for phases in petrological
908 calculations: an asymmetric multicomponent formulation. Contributions to Mineralogy and
909 Petrology, 145, 492–501.

910 Holland, T.J.B., and Powell, R. (2011) An improved and extended internally-consistent thermodynamic
911 dataset for phases of petrological interest, involving a new equation of state for solids. Journal of
912 Metamorphic Geology, 29, 333–383.

913 Howe, T.M., Lindsay, J.M., and Shane, P. (2015) Evolution of young andesitic-dacitic magmatic
914 systems beneath Dominica, Lesser Antilles. Journal of Volcanology and Geothermal Research, 297,
915 69–88.

916 Husen, A., Almeev, R.R., and Holtz, F. (2016) The effect of H_2O on pressure and multiple saturation
917 and liquid line of descent in basalt from the Shatsky Rise. Journal of Petrology, 57, 309–344.

918 Jennings, E.S., and Holland, T.J.B. (2015) A simple thermodynamic model for melting of peridotite in
919 the system NCFMASOCr. Journal of Petrology, 56, 869–892.

920 Juster, T. C., and Grove, T. L. (1989) Experimental constraints on the generation of FeTi basalts,
921 andesites, and riodacites at the Galapagos Spreading Center, 85˚W and 95˚W. Journal of
922 Geophysical Research, 94, 9251–9274.

923 Kawamoto, T. (1996) Experimental constraints on differentiation and H_2O abundance of calc-alkaline
924 magmas. Earth and Planetary Science Letters, 144, 577–589.

925 Kelemen, P.B., Kikawa, E., Miller, D.J., and Shipboard Scientific Party (2007) Leg 209 summary:
926 processes in a 20-km-thick conductive boundary layer beneath the Mid-Atlantic Ridge, 14°–16° N.
927 In P.B. Kelemen, E. Kikawa, D.J. Miller, Eds., Proceedings of the ODP, science results 209, p. 1-
928 33. College Station, TX., USA,

929 Kennedy, A.K., Grove, T.L., and Johnson, R.W. (1990) Experimental and major element constraints on
930 the evolution of lavas from Lihir Island, Papua New Guinea. Contributions to Mineralogy and
931 Petrology, 104, 722–734.

932 Kinzler, R.J., and Grove, T.L. (1992) Primary magmas of Mid-Ocean Ridge Basalts 1. Experiments
933 and methods. Journal of Geophysical Research, 97, 6885–6906.

934 Kopp, H., Weinzierl, W., Becel, A., Charvis, P., Evain, M., Flueh, E.R., Gailler, A., Galve, A., Hirn,
935 A., Kandilarov, A., Klaeschen, D., Laigle, M., Papenberg, C., Planert, L., and Roux, E. (2011) Deep
936 structure of the central Lesser Antilles Island Arc: relevance for the formation of continental crust.
937 Earth and Planetary Science Letters, 304, 121–134.

938 Lindsay, J., Stasiuk, M., and Shepherd, J. (2003) Geological history and potential hazards of the late-
939 Pleistocene to Recent Plat Pays volcanic complex, Dominica, Lesser Antilles. Bulletin of
940 Volcanology, 65, 201–220.

941 Lindsay, J., Trumbull, R.B., and Siebel, W. (2005) Geochemistry and petrogenesis of late Pleistocene
942 to Recent volcanism in Southern Dominica, Lesser Antilles. Journal of Volcanology and
943 Geothermal Research, 148, 253–294.

944 Lindsley, D. (1981) The formation of pigeonite on the join hedenbergite-ferrosilite at 11.5 kbar and 15
945 kbar: experiments and a solution model. American Mineralogist, 66, 1175–1182.

946 Lindsley, D. (1983) Pyroxene thermometry. American Mineralogist, 68, 477–493.

947 Loucks, R.R. (1996) A precise olivine-augite Mg-Fe exchange geothermometer. Contributions to
948 Mineralogy and Petrology, 125, 140–150.

949 Macdonald, R., Hawkesworth, C.J., and Heath, E. (2000) The Lesser Antilles volcanic chain: a study in
950 arc magmatism. Earth Science Review, 49, 1–76.

951 Mahood, G.A., and Baker, D.R. (1986) Experimental constraints on depths of fractionation of midly
952 alkali basalts and associated felsic rocks: Pantelleria, Strait of Sicily. Contributions to Mineralogy
953 and Petrology, 93, 251–264.

954 Mandler, B.E., Donnelly-Nolan, J.M., and Grove, T.L. (2014) Straddling the tholeiitic/calcalkaline
955 transition: the effects of modest amounts of water on magmatic differentiation at Newberry
956 Volcano, Oregon. Contributions to Mineralogy and Petrology, 168, 1066.

957 McGuire, A.V. (1994) Southern Basin and Range province crust-mantle boundary: evidence from
958 gabbroic xenoliths, Wikieup, Arizona. Journal of Geophysical Research, 99, 24263–24273[1SEP].

959 McGuire, A. V., and Mukasa, S. B. (1997) Magmatic modification of the uppermost mantle beneath the
960 Basin and Range to Colorado Plateau Transition Zone: Evidence from xenoliths, Wikieup, Arizona.
961 Contributions to Mineralogy and Petrology, 128, 52–65.

962 Melekhova, E., Blundy, J, Robertson, R., and Humphreys, M.C.S. (2015) Experimental evidence for
963 polybaric differentiation of primitive arc basalt beneath St. Vincent, Lesser Antilles. Journal of
964 Petrology, 56, 161–192.

965 Mikhail, E.M. (1976) Observations and Least Squares. Dun Donnelly, New York.

966 Molina, J.F., Moreno, J.A., Castro, A., Rodruiguez, C., and Fershtater, G.B. (2015) Calcic amphibole
967 thermobarometry in metamorphic and igneous rocks: new calibrations based on
968 plagioclase/amphibole Al-Si partitioning and amphibole-liquid Mg partitioning. Lithos, 232, 286–
969 305.

970 Mollo, S., Del Gaudio, P., Ventura, G., Iezzi, G., and Scarlato, P. (2010) Dependence of clinopyroxene
971 composition on cooling rate in basaltic magmas: implications for thermobarometry. Lithos, 118,
972 302–312.

973 Moore, G., and Carmichael, I.S.E. (1998) The hydrous phase equilibria (to 3 kbar) of an andesite and
974 basaltic andesite from western Mexico: constraints on water content and conditions of phenocryst
975 growth. Contributions to Mineralogy and Petrology, 130, 304–319.

976 Morimoto, N., Fabries, J., Ferguson, A.K., Ginzburg, I.V., Ross, M., Seifert, F.A., Zussman, J., Aoki,
977 K., and Gottardi, G. (1988) Nomenclature of pyroxenes. American Mineralogist, 73, 1123–1133.

978 Neave, D.A. and Putirka, K.D. (2017) A new clinopyroxene-liquid barometer, and implications for
979 magma storage pressures under Icelandic rift zones. American Mineralogist, 102, 777–794.

980 Nekvasil, H., Dondolini, A., Horn, J., Filiberto, J., Long, H., and Lindsley, D.H. (2004) The origin and
981 evolution of silica-saturated alkalic suites: an experimental study. Journal of Petrology, 45, 693–
982 721.

983 Nimis, P. (1995) A clinopyroxene geobarometer for basaltic systems based on crystals-structure
984 modeling. Contributions to Mineralogy and Petrology, 121, 115-125.

985 O'Neill, H.S.C., and Pownceby, M.I. (1993) Thermodynamic data from redox reactions at high
986 temperatures. I. An experimental and theoretical assessment of the electrochemical method using
987 stabilized zirconia electrolytes, with revised values for the Fe-“FeO”, Co-CoO, Ni-NiO and Cu-
988 Cu_2O oxygen buffers, and new data for the W-WO_2 buffer. Contributions to Mineralogy and
989 Petrology, 114, 296-314.

990 Parat, F., Streck, M.J., Holtz, F., and Almeev, R. (2014) Experimental study into the petrogenesis of
991 crystal-rich basaltic to andesitic magmas at Arenal volcano. Contributions to Mineralogy and
992 Petrology, 168, 1040.

993 Parsons, T., Howiem J.M., and Thompson, G.A. (1992) Seismic constraints on the nature of lower
994 crustal reflectors beneath the extending southern Transition Zone of the Colorado Plateau, Arizona.
995 Journal of Geophysical Research, 97, 12391–12407.

996 Pichavant, M., Martel, C., Bourdier, J-L., and Scaillet, B. (2002) Physical conditions, structure and
997 dynamics of a zoned magma chamber: Mount Pele (Martinique, Lesser Antilles arc). Journal of
998 Geophysical Research 107, doi:10.1029/2001JB000315.

999 Pichavant, M., and Macdonald, R. (2007) Crystallization of primitive basaltic magmas at crustal
1000 pressures and genesis of the calc-alkaline igneous suite: experimental evidence from St Vincent,
1001 Lesser Antilles arc. Contributions to Mineralogy and Petrology, 154, 535–558.

1002 Powell, R. (1985) Geothermometry and geobarometry: a discussion. Journal of the Geological Society,
1003 London, 142, 29–38.

1004 Powell, R., and Holland, T.J.B. (1988) An internally consistent thermodynamic dataset with
1005 uncertainties and correlations: 3: application methods, worked examples and a computer program.
1006 Journal of Metamorphic Geology, 6, 173–204.

1007 Powell, R., and Holland, T.J.B. (1993) On the formulation of simple mixing models for complex
1008 phases. American Mineralogist, 78, 1174–1180.

1009 Powell, R., and Holland, T.J.B. (1994) Optimal geothermometry and geobarometry. American
1010 Mineralogist, 79, 120–133.

1011 Powell, R., and Holland, T.J.B. (2008) On thermobarometry. Journal of Metamorphic Geology, 26,
1012 155–179.

1013 Putirka, K.D. (2008) Thermometers and barometers for volcanic systems. Reviews in Mineralogy and
1014 Geochemistry, 69, 61–120.

1015 Putirka, K. (2016a) Rates and styles of planetary cooling on Earth, Moon, Mars, and Vesta, using new
1016 models for oxygen fugacity, ferric-ferrous ratios, olivine-liquid Fe-Mg exchange, and mantle
1017 potential temperature. American Mineralogist, 101, 819–840.

1018 Putirka, K. (2016b) Amphibole thermometers and barometers for igneous systems and some

1019 implications for eruption mechanisms of felsic magmas at arc volcanoes. American Mineralogist,
1020 101, 841–858.

1021 Ridolfi, F., and Renzulli, A. (2012) Calcic amphiboles in calc-alkaline and alkaline magmas:
1022 thermobarometric and chemometric empirical equations valid up to 1,130°C and 2.2 GPa.
1023 Contributions to Mineralogy and Petrology, 163, 877–895.

1024 Sack, R.O., Walker, D., and Carmichael, I.S.E. (1987) Experimental petrology of alkalic lavas:
1025 constraints on cotectics of multiple saturation in natural basic liquids. Contributions to Mineralogy
1026 and Petrology, 96, 1–23.

1027 Scoates, J.S., Lo Cascio, M., Weis, D., and Lindsley, D.H. (2006) Experimental constraints on the
1028 origin and evolution of mildly alkalic basalts from the Kerguelen Archipelago, Southeast Indian
1029 Ocean. Contributions to Mineralogy and Petrology, 151, 582–599.

1030 Shejwalkar, A. and Coogan, L.A. (2013) Experimental calibration of the roles of temperature and
1031 composition in the Ca-in-olivine geothermometer at 0.1 MPa. Lithos, 177, 54–60.

1032 Sisson, T.W., and Grove, T.L. (1993) Experimental investigations of the role of H_2O in calc-alkaline
1033 differentiation and subduction zone magmatism. Contributions to Mineralogy and Petrology 113,
1034 143–166.

1035 Stamper, C.C., Melekhova, E., Blundy, J.D., Arculus, R.J., Humphreys, M.C.S., and Brooker, R.A.
1036 (2014a) Oxidised phase relations of a primitive basalt from Grenada, Lesser Antilles. Contributions
1037 to Mineralogy and Petrology, 167, 1-20.

1038 Stamper, C.C., Blundy, J.D., Arculus, R.J., and Melekhova, E. (2014b) Petrology of plutonic xenoliths
1039 and volcanic rocks from Grenada, Lesser Antilles. Journal of Petrology, 55, 1353–1387.

1040 Streckeisen, A. (1976) To each plutonic rock its proper name. Earth Science Reviews, 12, 1–33.

1041 Takagi, D., Sato, H., and Nakagawa, M. (2005) Experimental study of a low-alkali tholeiite at 1–5
1042 kbar: optimal condition for the crystallization of high-An plagioclase in hydrous arc tholeiite.
1043 Contributions to Mineralogy and Petrology, 149, 527–540.

1044 Tollan, P., Bindeman, I., and Blundy, J. (2012) Cumulate xenoliths from St. Vincent, Lesser Antilles
1045 Island Arc: a window into upper crustal differentiation of mantle-derived basalts. Contributions to
1046 Mineralogy and Petrology, 163, 189–208.

1047 Toplis, M., and Carroll, M.R. (1995) An experimental study of the influence of oxygen fugacity on Fe-
1048 Ti oxide stability, phase relations, and mineral-melt equilibria in ferro-basaltic systems. Journal of
1049 Petrology, 36, 1137–1170.

1050 Turnock A.C., and Lindsley D.H. (1981) Experimental determination of pyroxene solvi for ≤1 kbar at
1051 900 and 1000 C. Canadian Mineralogist, 19, 255–267.

1052 Wagner, T.P., Donnelly-Nolan, J.M., and Grove, T.L. (1995) Evidence of hydrous differentiation and
1053 crystal accumulation in the low-MgO, high-Al_2O_3 Lake Basalt from Medicine Lake volcano,
1054 California. Contributions to Mineralogy and Petrology, 121, 201–216.

1055 Wells, P.R.A. (1977) Pyroxene thermometry in simple and complex systems. Contributions to
1056 Mineralogy and Petrology, 62, 129–139.

1057 White, R.W., Powell, R., Holland, T.J.B., Johnson, T.E., and Green, E.C.R. (2014) New mineral
1058 activity–composition relations for thermodynamic calculations in metapelitic systems. Journal of
1059 Metamorphic Geology, 32, 261–286.

1060 Wilshire, H.G. (1990) Lithology and evolution of the crust-mantle boundary region in the southwestern
1061 Basin and Range province. Journal of Geophysical Research, 95, 649–665.

1062

Figure captions

Figure 1. *P-T* conditions of phase equilibrium experiments in basaltic and peridotitic systems that contain at least olivine, clinopyroxene and plagioclase in their phase assemblages. Source references for this database are reported in Supplementary Material 1.

Figure 2. Composition of the mineral phases used for avP calculations on experimental and natural samples. (**a**) Pyroxene quadrilateral projection (Morimoto 1988). (**b**) Forsterite content in olivine plotted vs anorthite content in plagioclase. (**c**) Trivalent cation plot for spinels [Fe^{3+} = $Fe^{3+}/(Fe^{3+}+Al+Cr)$, Al = $Al/(Fe^{3+}+Al+Cr)$, Cr = $Cr/(Fe^{3+}+Al+Cr)$].

Figure 3. Variation of Al^{IV} in clinopyroxene with pressure in the experimental database. Note the wide range of Al^{IV} for the experiments at 0.001 kbar, which is larger than the variations for the entire dataset at higher pressures.

Figure 4. Independent set of reactions and avP results at T_0 = 870 ˚C for the spinel + clinopyroxene + olivine + plagioclase (SCOlP) assemblage in olivine-gabbronorite DC90 (Dominica, Lesser Antilles). The reactions are linearised at T_0 = 870 ˚C and P_0 = 4 kbar. In the minimization procedure, avP makes minimal adjustments to the enthalpies and activities of end-members, given their covariance matrices, in order for the reactions to coincide at $\overline{P}$. Reactions derived from the initial input data, i.e. the dataset enthalpies and the activities at the measured compositions, are shown as solid curves. Reactions after minimization are shown as dashed curves. The box at the bottom shows the pressures initially obtained from each individual reaction with their associated uncertainties, at T_0 = 870 ˚C. For end-member abbreviations see Table 2. A detailed step-by-step demonstration of the same calculation is reported in the Supplementary Material 2.

Figure 5. Results of avP calculations on the refined database of experiments containing the subset SCOlP in their run products. Calculations have been performed with either (**a**) SCOlP equilibria (i.e., 6 reactions) or (**b**) COlP equilibria (3 reactions), using the thermodynamic model refined in this work. Error bars are $\sigma_{\bar{P}}$ (see text). The labels on the x-axes are the experiment index numbers, ordered as in the Supplementary Material 1 (i.e., increasing P_{exp})

Figure 6. Residuals in calculated $\overline{P}$ relative to P_{exp}, for SCOlP equilibria, plotted vs. (**a**) T_{exp}, (**b**) spinel $Fe^{3+}/[Fe^{3+}+Al+Cr]$ and (**c**) clinopyroxene mg#. Dataset and symbols as in Fig. 5.

Figure 7. Results of multiple avP calculations at different temperatures T_0 for the experimental sample ShR658 (Husen et al. 2016). $P_0 = P_{exp}$ for all the calculations. The temperature dependence of the calculated pressure ($d\overline{P}/dT_0$) for this sample is indicated in the top box. $T\sigma_{fit}$ is the value of T_0 that produces the avP result with the lowest σ_{fit} ($\overline{P}\sigma_{fit}$). Note, with reference to the uncertainty envelope (grey envelope in the top box), that outside the T range in which the χ^2 test is passed, the uncertainty is multiplied by σ_{fit}.

Figure 8. Temperature dependence of avP ($d\overline{P}/dT_0$) plotted vs. calculated pressures (at $T_0 = T_{exp}$), for the selected experimental dataset used in this work. The higher the calculated value of $\overline{P}$, the less sensitive this value is to the choice of T_0.

Figure 9. Temperature estimates derived by minimising σ_{fit} ($T\sigma_{fit}$) for the experimental dataset and their effect on the calculated $\overline{P}$. (**a**) Comparison between $T\sigma_{fit}$ and the true temperature T_{exp}. (**b,c**) Test of $\overline{P} \pm \sigma_{\bar{P}}$ calculated using either (**b**) $T_0 = T\sigma_{fit}$ or (**c**) $T_0 = T_{exp}$. In (c), experiments shown in black are those for which $T\sigma_{fit}$ cannot be estimated, as no minimum in σ_{fit} as a function of T_0 can be identified. In all cases $P_0 = P_{exp}$. SEE: - Standard Error of Estimate; Pred: - percentage of calculations that predict P_{exp} within $\sigma_{\bar{P}}$.

1116

1117 **Figure 10.** Photomicrographs (plain polarised light) of the selected xenoliths from Dominica,
1118 with locations of the microprobe analyses used for avP calculations. Results of avP calculations
1119 with SCOlP equilibria are also reported in the boxes at the bottom-left corners.

1120

1121 **Figure 11.** Calculated depths for the three xenoliths from Dominica, Lesser Antilles, compared
1122 with the seismic model of Kopp et al. (2011). Depths calculated as in Table 3. Numbers in the
1123 figure refer to v_p velocities (km/s).

1124

1125 **Figure 12.** Calculated depths (as Table 3) for the ol-gabbro and pl-peridotite xenoliths from
1126 Wikieup, shown in comparison to the density profile across the Arizona Transition Zone (Bashir
1127 et al. 2011). BR – Basin and Range; CP – Colorado Plateau.

Deposit items

Supplementary Material 1: Experimental database

Supplementary Material 2: Example of avP calculation and diagnostics

Supplementary Material 3: Thermodynamic dataset and activity-composition models

Supplementary Material 4: Uncertainties on compositional variables for the experimental dataset

Supplementary Material 5: Electron microprobe analyses

Supplementary Material 6: AvP calculations with COlP equilibria on the experimental database

Supplementary Material 7: Correlation matrixes of the reactions

Supplementary Material 8: Description of xenoliths from Dominica, Lesser Antilles

Table 1. Abbreviations used in this work

SCOlP	Spinel + Clinopyroxene + Olivine + Plagioclase, where 'spinel' may refer to either magnetite or Cr/Al-spinel.
COlP	Clinopyroxene + Olivine + Plagioclase
apfu	atoms per formula unit
mg#	$Mg/(Mg+Fe^{2+})$
NNO	nickel-nickel oxide buffer
P_{exp}, T_{exp}	measured pressure, temperature of the experiment
P_0, T_0	initial guesses of pressure and temperature
ΔG_r^o	Gibbs free energy difference in kJ for the reaction *r* among the pure end-members
ν_i	reaction coefficient for end-member *i*, at *P, T*
μ_i	total chemical potential for end-member *i*
μ_i^0	chemical potential of the pure end-member at *P, T*
R	gas constant (0.0083144 kJ/K·mole)
$W_{(m,n)}^j$	pairwise interaction energy representing non-ideal enthalpy of mixing between end-members *m* and *n* in phase *j*.
a_i	activity of end-member *i*
K_r	equilibrium constant for reaction *r*
ΔH_r	enthalpy change for reaction *r*, at *P, T*
ΔS_r	entropy change for reaction *r*, at *P, T*
ΔV_r	volume change for reaction *r*, at *P, T*
P_r	pressure at T_0 for reaction *r*
$\overline{P}$	average pressure (at T_0) calculated through the avP algorithm
$\sigma_{\bar{P}}$	calculated 1σ uncertainty for $\overline{P}$
σ_{fit}	diagnostic value that measures the appropriateness of the average, with σ_{fit}^2 distributed as χ^2.
e_i^*	uncertainty-normalized residuals in log (activity) for end-member *i*
H_i^*	uncertainty-normalized residuals in the enthalpy for end-member *i*
h_i	hat value, i.e., degree of influence of the end-member *i* on the least-square results
$T_{\sigma_{fit}}$	T_0 that produces the avP result with the minimum value of σ_{fit}
SEE	standard error of the estimate

Table 2. Solid solutions and compositional end-members used in this work. Columns SCOlP and COlP show which end-members are included in the avP calculations using the SCOlP and COlP equilibria, respectively. End-members are described in the Holland and Powell (2011) dataset, using the abbreviations shown, with the exception of cenh and cfs.

Solid solution	End-member	Abbreviation	Formula	SCOlP	COlP
Olivine	forsterite	fo	Mg_2SiO_4	x	x
	fayalite	fa	Fe_2SiO_4	x	x
Spinel	spinel	sp	$MgAl_2O_4$	x	
	hercynite	herc	$FeAl_2O_4$	x	
	magnetite	mt	Fe_3O_4	x	
	picrochromite*	picr	$MgCr_2O_4$		
	ulvöspinel*	usp	Fe_2TiO_4		
Clinopyroxene	diopside	di	$CaMgSi_2O_6$	x	
	clinoenstatite	cenh	$Mg_2Si_2O_6$	x	x
	clinoferrosilite	cfs	$Fe_2Si_2O_6$	x	x
	jadeite	jd	$NaAlSi_2O_6$	x	x
	acmite	acm	$NaFeSi_2O_6$	x	
	Ca-tschermak	cats	$CaAl_2SiO_6$	x	x
Plagioclase	high-albite	abh	$NaAlSi_3O_8$	x	x
	anorthite	an	$CaAl_2Si_2O_8$	x	x
	sanidine*	san	$KAlSi_3O_8$		

* end-members for which balanced reactions cannot be written. Note that these end-members are still considered in the calculations of the activities of the end-members involved in the reactions.

Table 3. Results of avP calculations for the xenoliths from Dominica and Wikieup. For all the calculations, P_0 = 4.0 kbar and $T_0 = T\sigma_{fit}$. Uncertainties on compositional variables have been propagated from analytical errors, with the corrections adopted in this work (see Supplementary Material 5). $T_{cpx\text{-}opx}$ refers to temperature calculated using eq. 37 in Putirka (2008). Depths of the xenoliths have been calculated from the estimated pressures, assuming an average density ($\bar{\rho}$) of the overlying crust of 2800 g/cm^3.

Sample	$T_{cpx\text{-}opx}$ (˚C)	$T\sigma_{fit}$ (˚C)	SCOlP equilibria $\overline{P}$ kbar	$\sigma_{\bar{P}}$ kbar	σ_{fit}	depth km	COlP equilibria $\overline{P}$ kbar	$\sigma_{\bar{P}}$ kbar	σ_{fit}
Dominica:									
DC90	-	870	3.58	0.91	0.81	13.0 ± 3.3	4.21	0.98	0.36
DC91	896	910	1.94	1.09	0.94	7.1 ± 4.0	2.81	1.23	0.40
DC93a	-	980	2.67	1.35	1.48	9.7 ± 4.9	3.66	0.97	0.92
DC93b	-	1000	2.81	1.55	1.54	10.2 ± 5.6	3.76	1.41	1.31
Wikieup:									
WK2-9	887	940	6.53	0.97	0.40	23.8 ± 3.5	6.55	0.99	0.54
WK2-49a	-	1000	6.20	1.00	0.74	22.6 ± 3.6	6.19	1.20	1.17
WK1-24	-	1150	6.54	0.95	0.55	23.8 ± 3.5	6.46	0.99	0.84
WK1-63	953	1150	6.88	0.97	0.48	25.0 ± 3.5	6.86	1.00	0.73

Figure 1

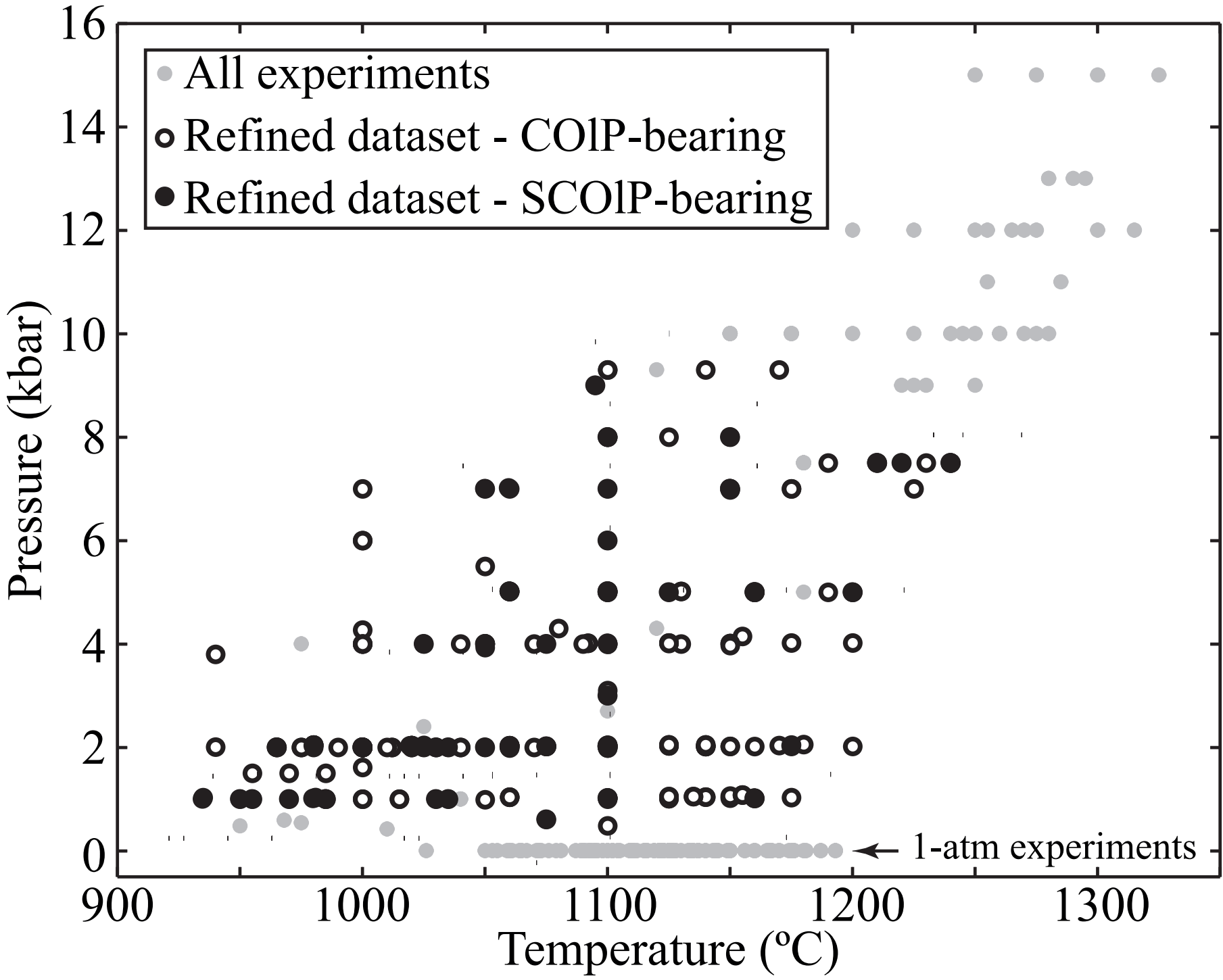
All experiments
Refined dataset - COlP-bearing
Refined dataset - SCOlP-bearing
1-atm experiments
Pressure (kbar)
Temperature (ºC)
0
2
4
6
8
10
12
14
16
900
1000
1100
1200
1300

Figure 2

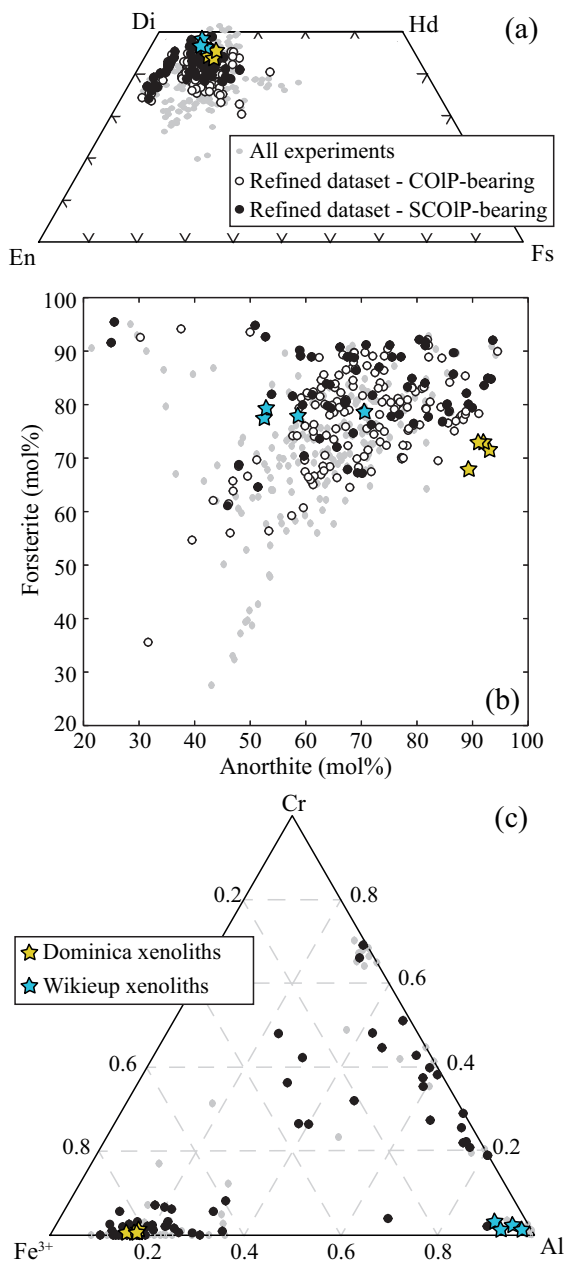
Di
Hd
(a)
All experiments
Refined dataset - COlP-bearing
Refined dataset - SCOlP-bearing
En
Fs
Forsterite (mol%)
Anorthite (mol%)
(b)
Cr
(c)
Dominica xenoliths
Wikieup xenoliths
Fe3+
Al

Figure 3

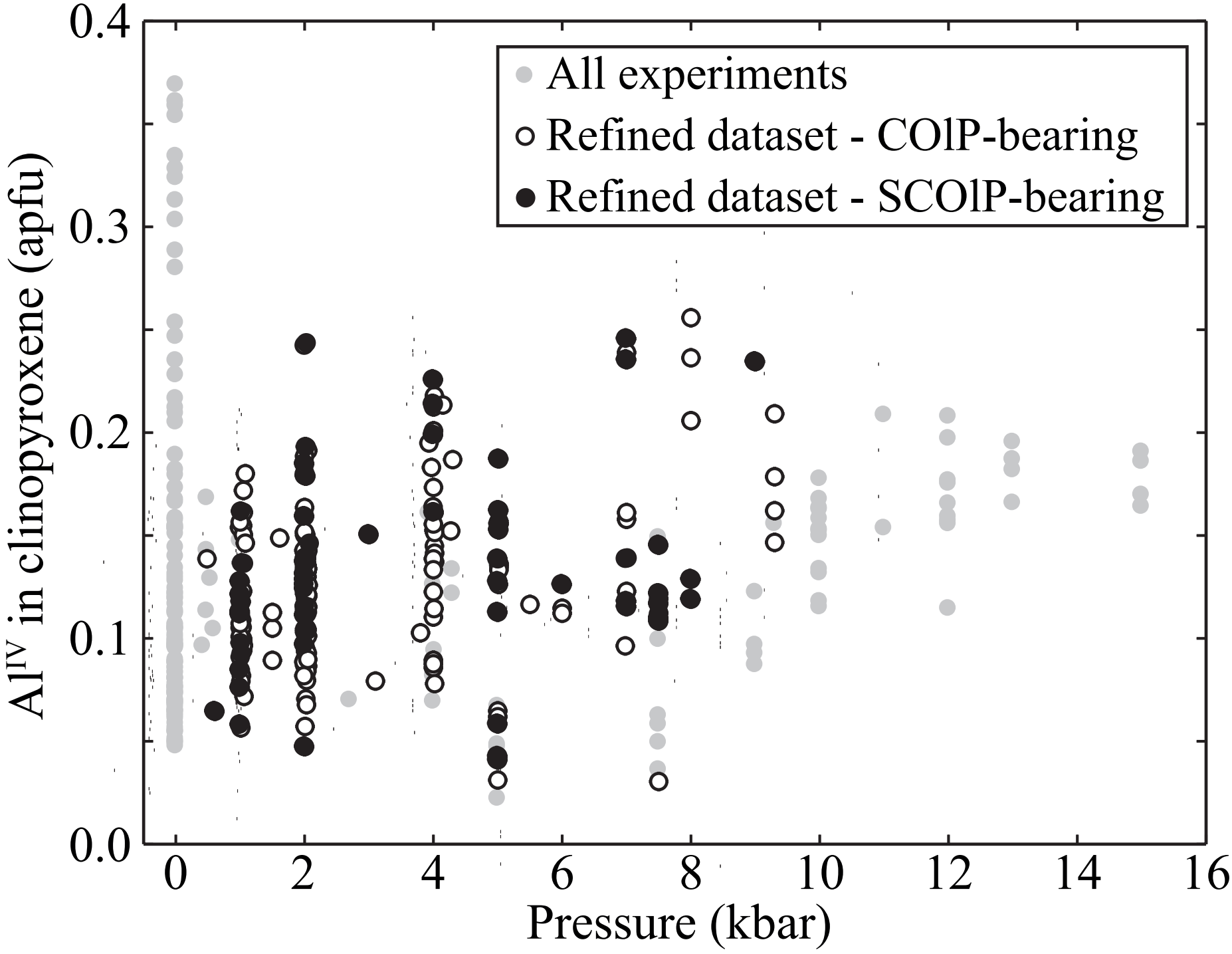
All experiments
Refined dataset - COlP-bearing
Refined dataset - SCOlP-bearing
Al^{IV} in clinopyroxene (apfu)
Pressure (kbar)
0.0
0.1
0.2
0.3
0.4
0
2
4
6
8
10
12
14
16

Figure 4

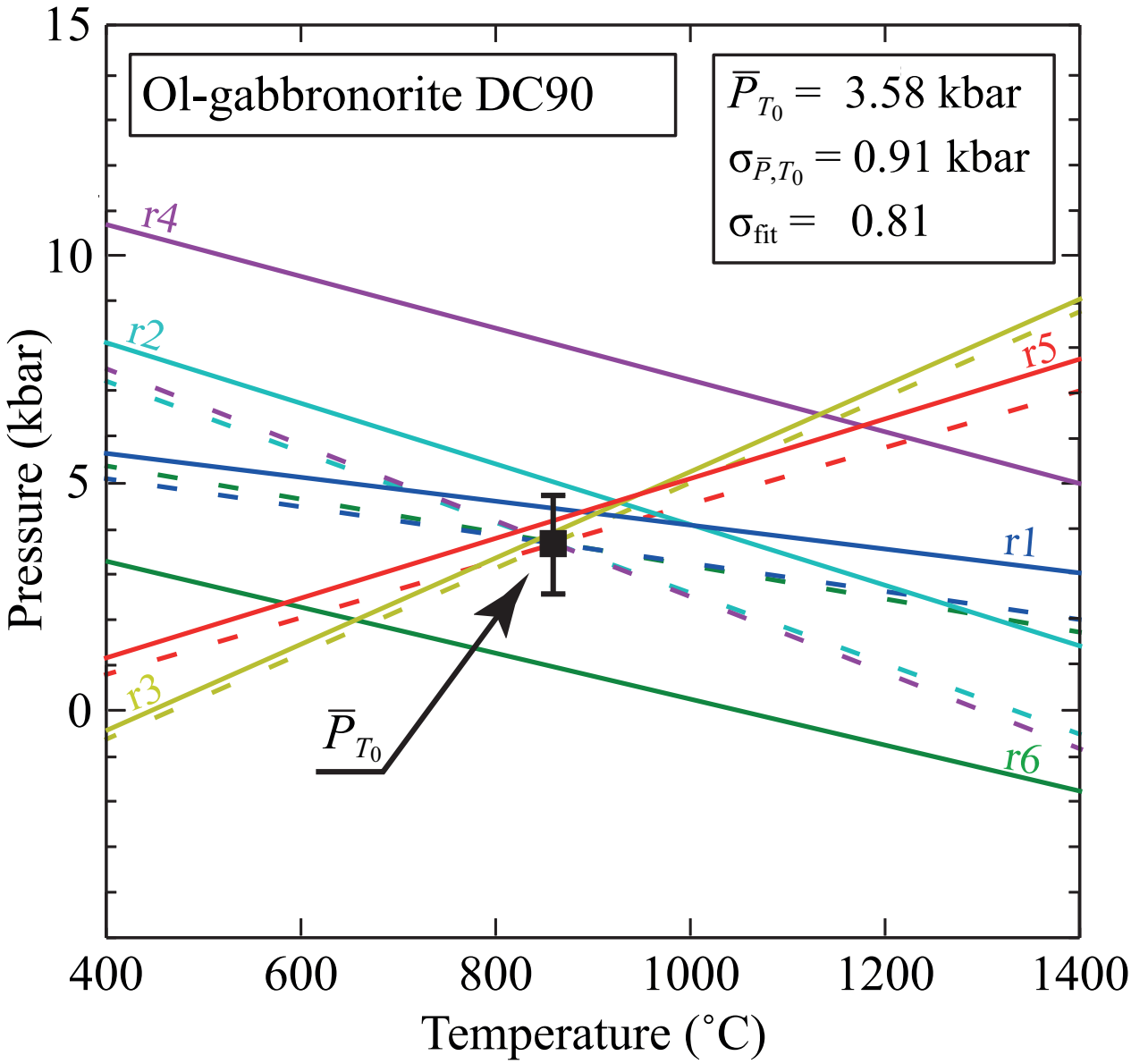

Reactions	P_r (kbar)
r1) fo + an = cenh + cats	4.3 ± 1.4
r2) fa + an = cfs + cats	4.8 ± 1.6
r3) fo + abh = cenh + jd	4.0 ± 1.3
r4) di + an + sp = cenh + 2cats	8.1 ± 4.4
r5) fa + abh + 2sp = cenh + jd + 2herc	4.3 ± 7.2
r6) 2fa + 2abh + mt = 2cfs + 2acm + herc	0.8 ± 2.4

Figure 5

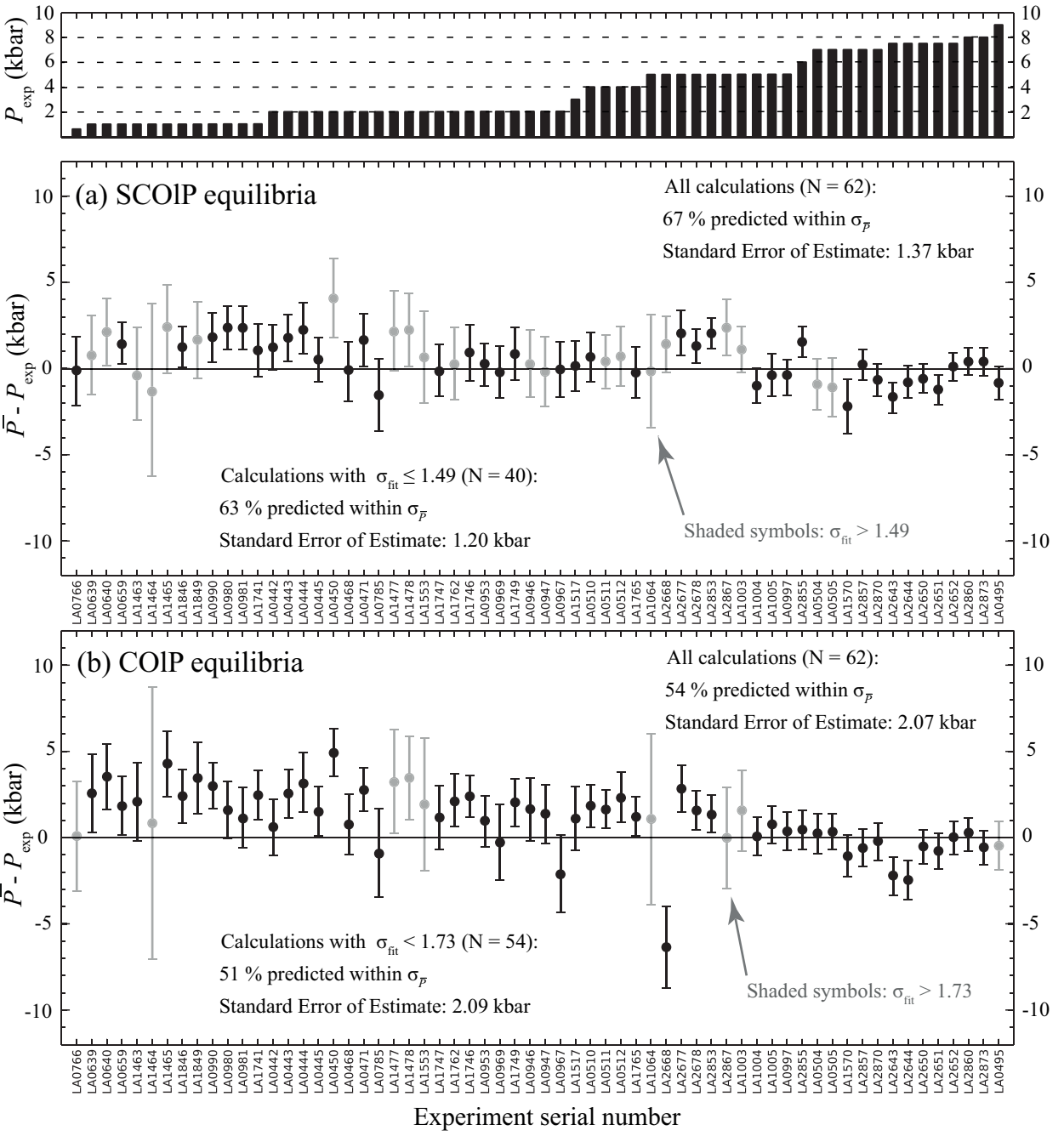
P_{exp} (kbar)
(a) SCOlP equilibria
All calculations (N = 62):
67 % predicted within $\sigma_{\bar{P}}$
Standard Error of Estimate: 1.37 kbar
$\bar{P}$ - P_{exp} (kbar)
Calculations with $\sigma_{fit} \leq 1.49$ (N = 40):
63 % predicted within $\sigma_{\bar{P}}$
Standard Error of Estimate: 1.20 kbar
Shaded symbols: $\sigma_{fit} > 1.49$
(b) COlP equilibria
All calculations (N = 62):
54 % predicted within $\sigma_{\bar{P}}$
Standard Error of Estimate: 2.07 kbar
Calculations with $\sigma_{fit} < 1.73$ (N = 54):
51 % predicted within $\sigma_{\bar{P}}$
Standard Error of Estimate: 2.09 kbar
Shaded symbols: $\sigma_{fit} > 1.73$
LA0766 LA0639 LA0640 LA0659 LA1463 LA1464 LA1465 LA1846 LA1849 LA0990 LA0980 LA0981 LA1741 LA0442 LA0443 LA0444 LA0445 LA0450 LA0468 LA0471 LA0785 LA1477 LA1478 LA1553 LA1747 LA1762 LA1746 LA0953 LA0969 LA1749 LA0946 LA0947 LA0967 LA1517 LA0510 LA0511 LA0512 LA1765 LA1064 LA2668 LA2677 LA2678 LA2853 LA2867 LA1003 LA1004 LA1005 LA0997 LA2855 LA0504 LA0505 LA1570 LA2857 LA2870 LA2643 LA2644 LA2650 LA2651 LA2652 LA2860 LA2873 LA0495
Experiment serial number

Figure 6

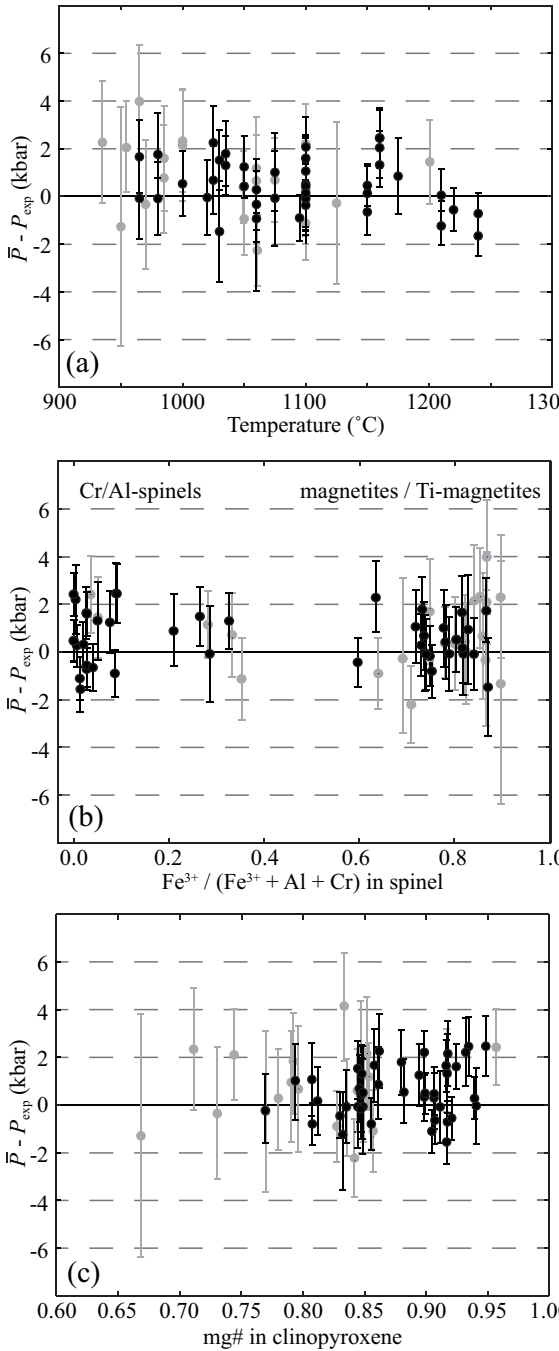
$\bar{P}$ - P_{exp} (kbar)
6
4
2
0
-2
-4
-6
(a)
900
1000
1100
1200
1300
Temperature (˚C)
Cr/Al-spinels
magnetites / Ti-magnetites
(b)
0.0
0.2
0.4
0.6
0.8
1.0
Fe^{3+} / (Fe^{3+} + Al + Cr) in spinel
(c)
0.60
0.65
0.70
0.75
0.80
0.85
0.90
0.95
1.00
mg# in clinopyroxene

Figure 7

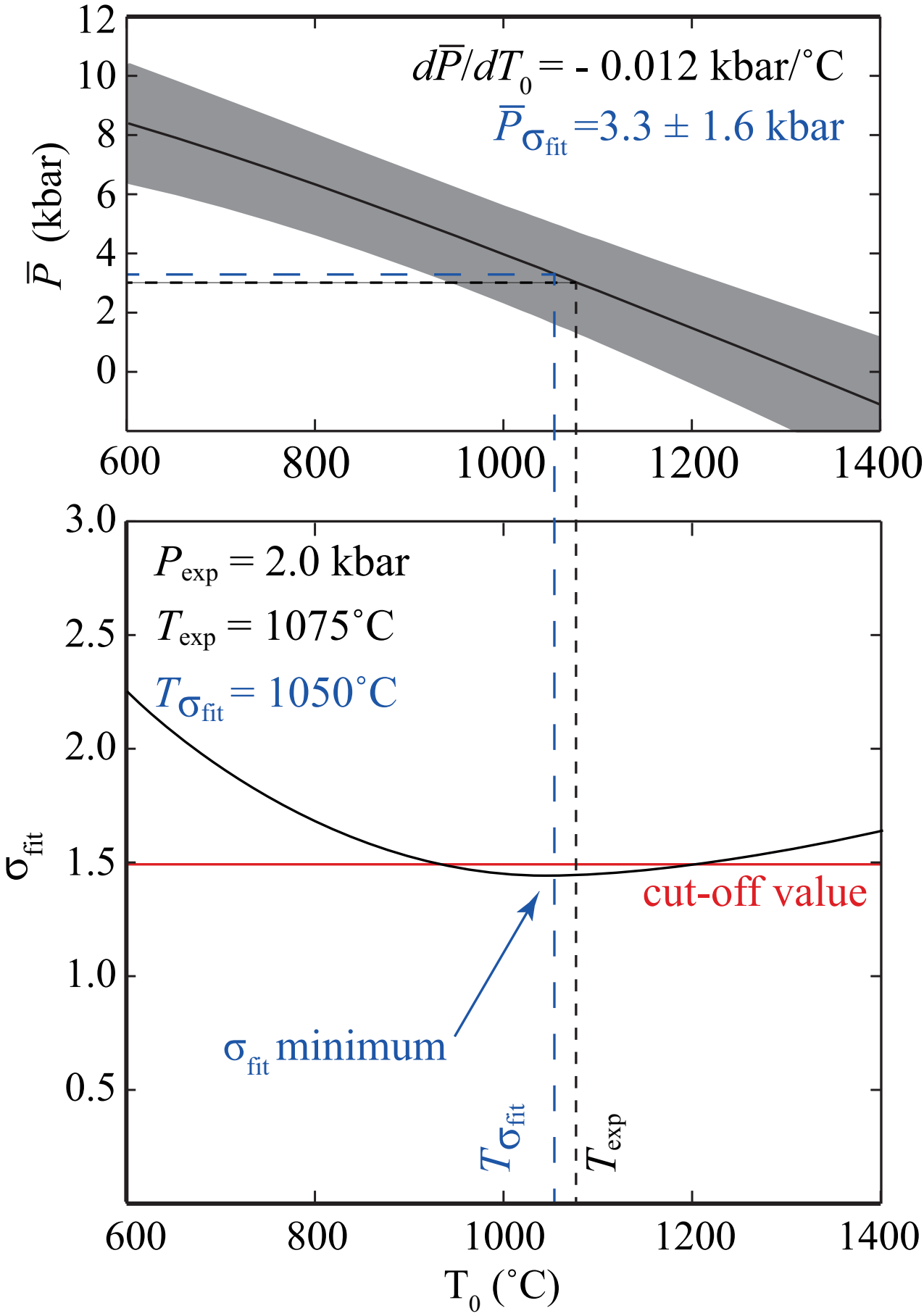
$d\bar{P}/dT_0$ = - 0.012 kbar/°C
$\bar{P}_{\sigma_{fit}}$ =3.3 ± 1.6 kbar
$\bar{P}$ (kbar)
P_{exp} = 2.0 kbar
T_{exp} = 1075°C
$T_{\sigma_{fit}}$ = 1050°C
σ_{fit}
cut-off value
σ_{fit} minimum
$T_{\sigma_{fit}}$
T_{exp}
T_0 (°C)

Figure 8

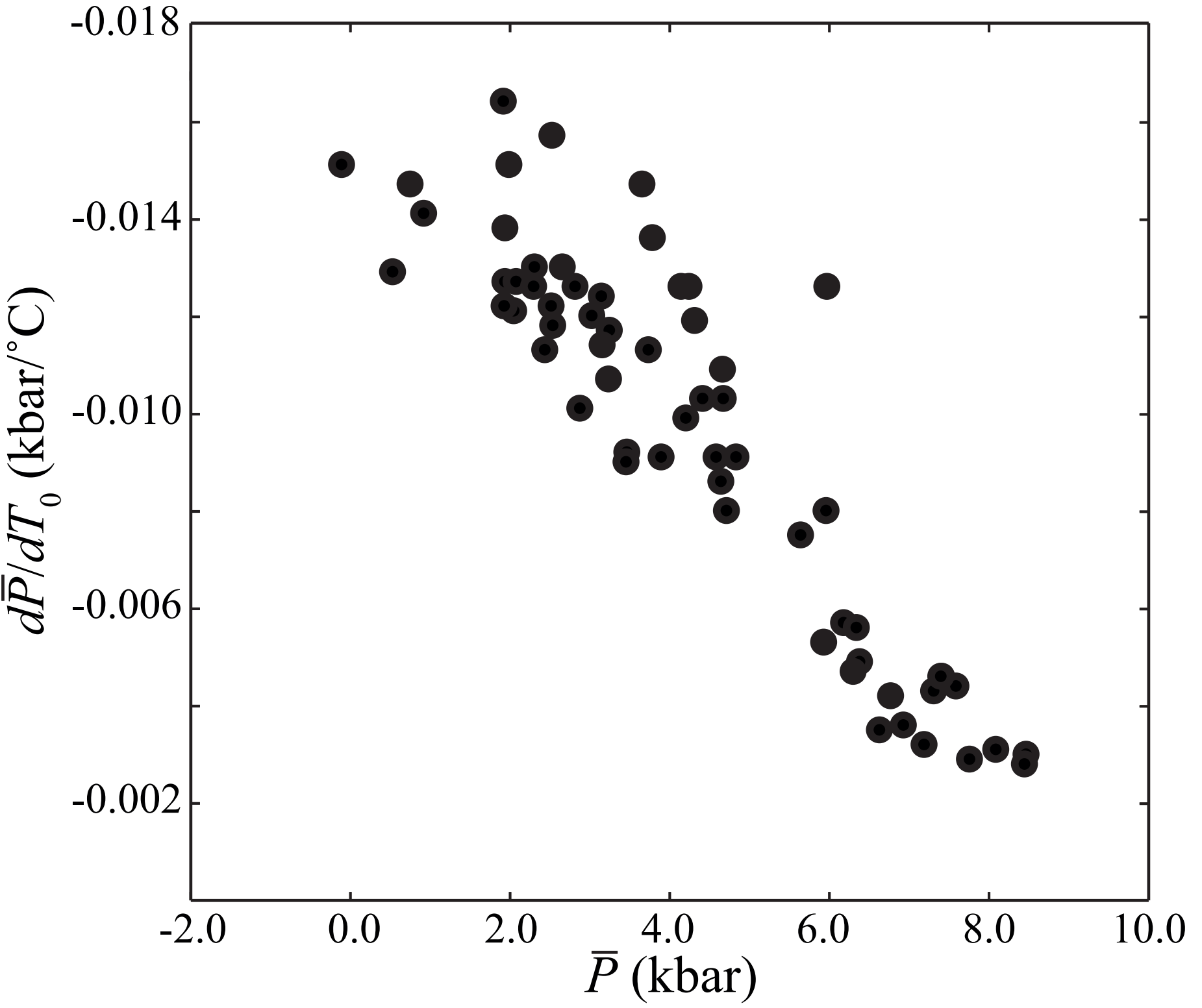
-0.018
-0.014
-0.010
-0.006
-0.002
$d\bar{P}/dT_0$ (kbar/°C)
-2.0
0.0
2.0
4.0
6.0
8.0
10.0
$\bar{P}$ (kbar)

Figure 9

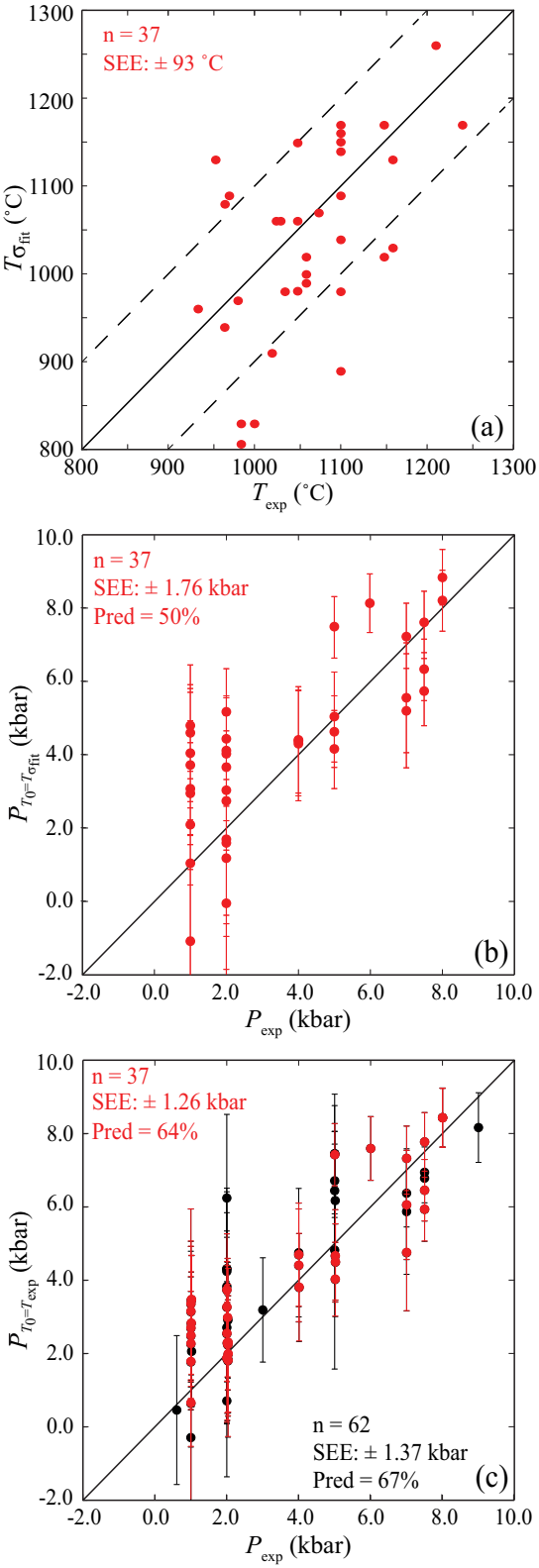
n = 37
SEE: ± 93 ˚C
(a)
$T_{\sigma_{fit}}$ (˚C)
T_{exp} (˚C)
n = 37
SEE: ± 1.76 kbar
Pred = 50%
(b)
$P_{T_0=T_{\sigma_{fit}}}$ (kbar)
P_{exp} (kbar)
n = 37
SEE: ± 1.26 kbar
Pred = 64%
n = 62
SEE: ± 1.37 kbar
Pred = 67%
(c)
$P_{T_0=T_{exp}}$ (kbar)
P_{exp} (kbar)

Figure 10

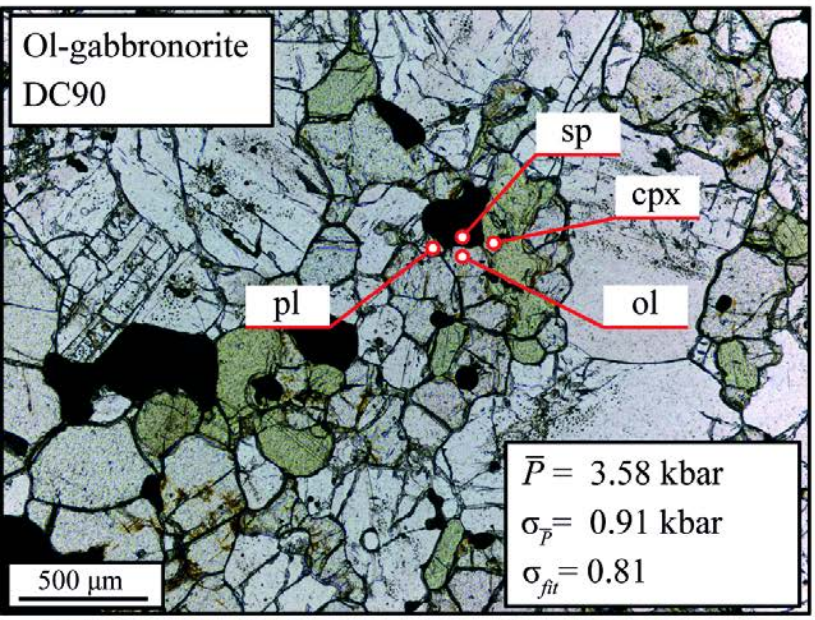
Ol-gabbronorite
DC90
sp
cpx
pl
ol
$\overline{P}$ = 3.58 kbar
$\sigma_{\overline{P}}$ = 0.91 kbar
σ_{fit} = 0.81
500 µm

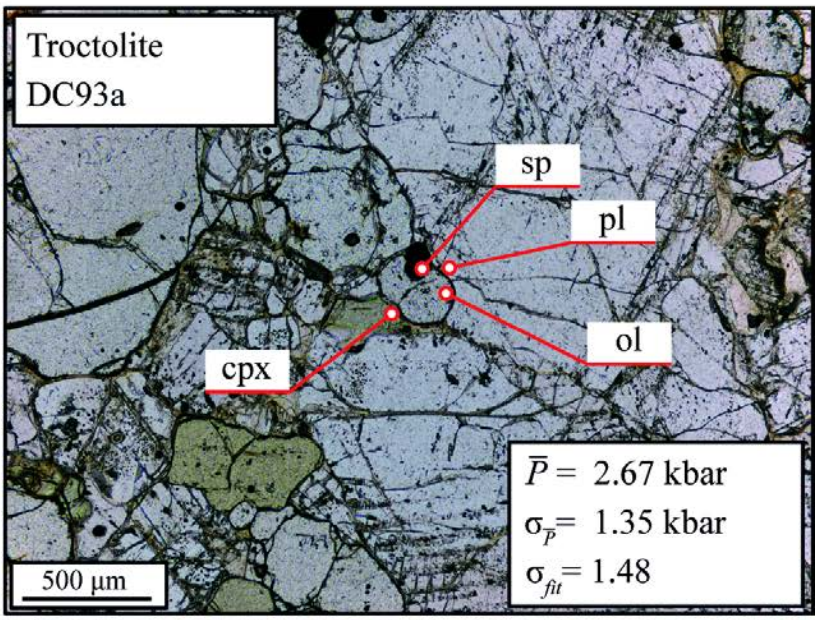
Troctolite
DC93a
sp
pl
ol
cpx
$\overline{P}$ = 2.67 kbar
$\sigma_{\overline{P}}$ = 1.35 kbar
σ_{fit} = 1.48
500 µm

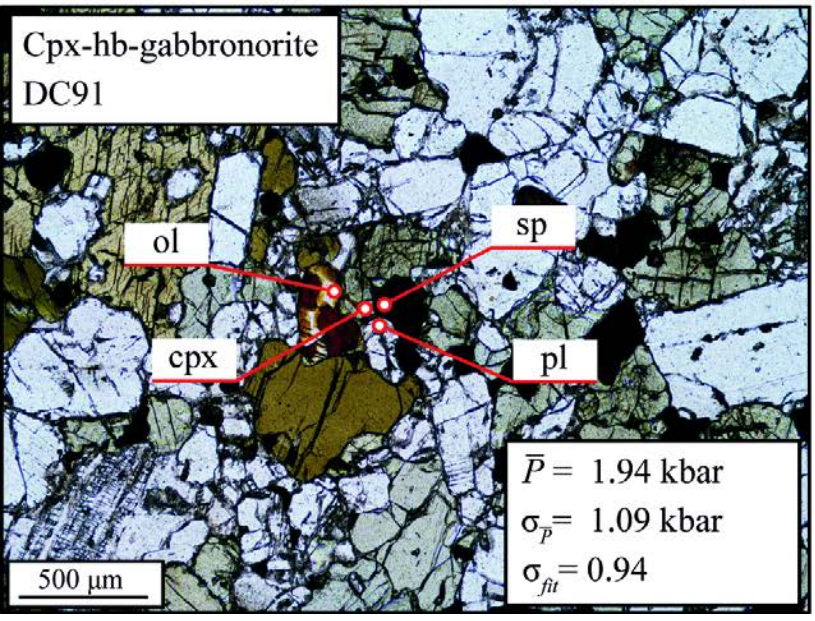
Cpx-hb-gabbronorite
DC91
ol
sp
cpx
pl
$\overline{P}$ = 1.94 kbar
$\sigma_{\overline{P}}$ = 1.09 kbar
σ_{fit} = 0.94
500 µm

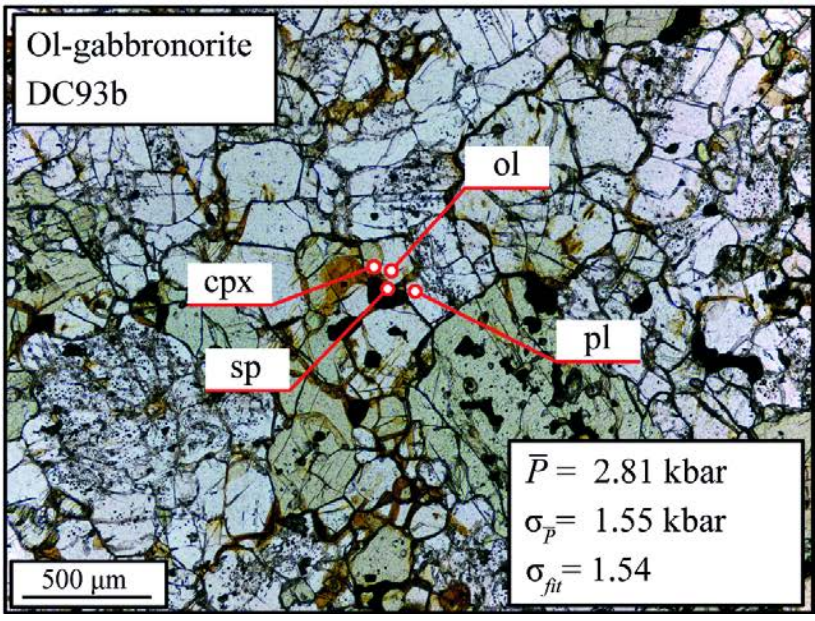
Ol-gabbronorite
DC93b
ol
cpx
sp
pl
$\overline{P}$ = 2.81 kbar
$\sigma_{\overline{P}}$ = 1.55 kbar
σ_{fit} = 1.54
500 µm

Figure 11

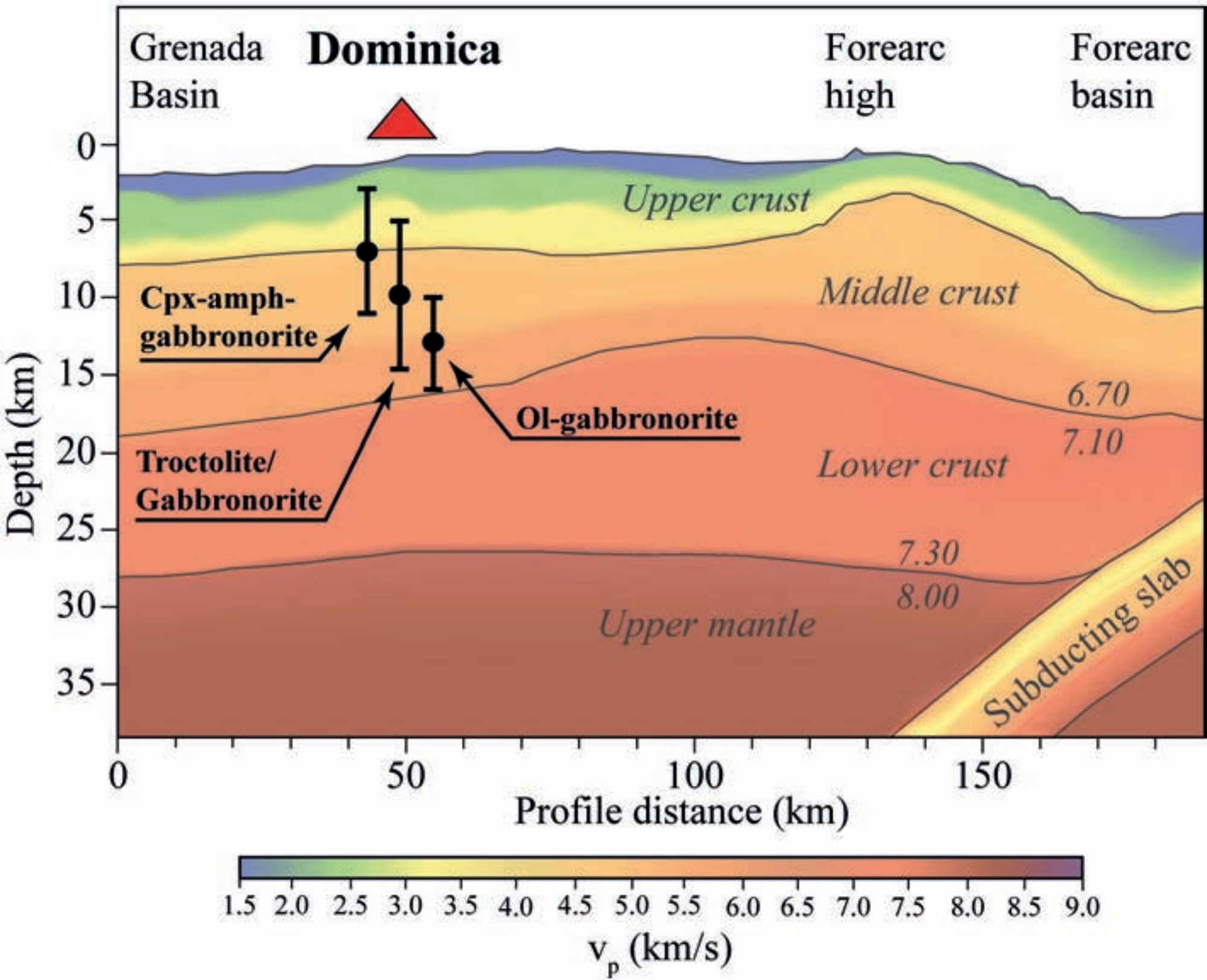
Grenada Basin
Dominica
Forearc high
Forearc basin
Upper crust
Middle crust
Lower crust
Upper mantle
Cpx-amph-gabbronorite
Ol-gabbronorite
Troctolite/ Gabbronorite
6.70
7.10
7.30
8.00
Subducting slab
Depth (km)
0
5
10
15
20
25
30
35
0
50
100
150
Profile distance (km)
1.5 2.0 2.5 3.0 3.5 4.0 4.5 5.0 5.5 6.0 6.5 7.0 7.5 8.0 8.5 9.0
v_p (km/s)

Figure 12

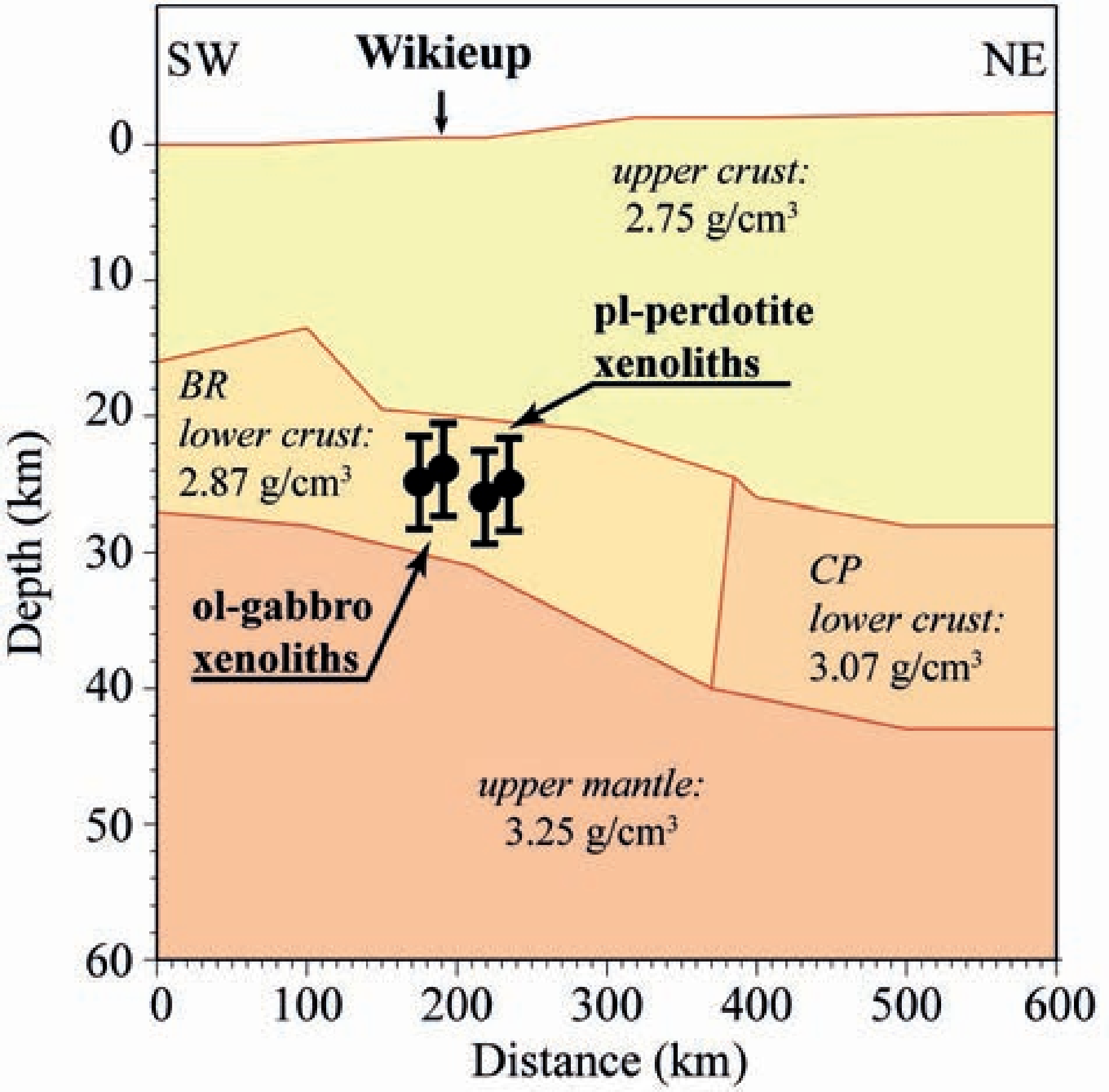
SW
Wikieup
NE
0
10
20
30
40
50
60
Depth (km)
upper crust:
2.75 g/cm3
pl-perdotite
xenoliths
BR
lower crust:
2.87 g/cm3
ol-gabbro
xenoliths
CP
lower crust:
3.07 g/cm3
upper mantle:
3.25 g/cm3
0
100
200
300
400
500
600
Distance (km)